Predator-informed looming stimulus experiments reveal how large filter feeding whales capture highly maneuverable forage fish

David E. Cade[a,1,2], Nicholas Carey[a,2,3], Paolo Domenici[b], Jean Potvin[c], and Jeremy A. Goldbogen[a]

[a]Hopkins Marine Station, Department of Biology, Stanford University, Pacific Grove, CA 93950; [b]Istituto per lo studio degli impatti Antropici e Sostenibilità in ambiente marino, Consiglio Nazionale delle Ricerche, IAS-CNR, 09170, Torregrande, Oristano, Italy; and [c]Department of Physics, Saint Louis University, St. Louis, MO 63103

Edited by James A. Estes, University of California, Santa Cruz, CA, and approved November 13, 2019 (received for review June 27, 2019)

The unique engulfment filtration strategy of microphagous rorqual whales has evolved relatively recently (<5 Ma) and exploits extreme predator/prey size ratios to overcome the maneuverability advantages of swarms of small prey, such as krill. Forage fish, in contrast, have been engaged in evolutionary arms races with their predators for more than 100 million years and have performance capabilities that suggest they should easily evade whale-sized predators, yet they are regularly hunted by some species of rorqual whales. To explore this phenomenon, we determined, in a laboratory setting, when individual anchovies initiated escape from virtually approaching whales, then used these results along with in situ humpback whale attack data to model how predator speed and engulfment timing affected capture rates. Anchovies were found to respond to approaching visual looming stimuli at expansion rates that give ample chance to escape from a sea lion-sized predator, but humpback whales could capture as much as 30–60% of a school at once because the increase in their apparent (visual) size does not cross their prey's response threshold until after rapid jaw expansion. Humpback whales are, thus, incentivized to delay engulfment until they are very close to a prey school, even if this results in higher hydrodynamic drag. This potential exaptation of a microphagous filter feeding strategy for fish foraging enables humpback whales to achieve 7× the energetic efficiency (per lunge) of krill foraging, allowing for flexible foraging strategies that may underlie their ecological success in fluctuating oceanic conditions.

predator/prey | looming stimulus | humpback whale | fish feeding | attack kinematics

In both terrestrial and aquatic ecosystems, maximum locomotor speed generally increases, but maneuverability decreases with increasing body sizes (1, 2). For pursuit predators chasing small prey at predator/prey size ratios of 10^0–10^1, this scaling property implies that speed advantages inherent in the predator's larger size can be counteracted by the prey's maneuverability advantages (2–4). At greater predator–prey size ratios (~10^2) that commonly occur in 3D, open ocean environments, whole-body acceleration attacks are generally suboptimal due to the maneuverability of the prey, and predators must use supplemental strategies, such as ambush, group coordination, or acceleration of smaller appendages to overcome their prey's escape abilities (2, 4, 5). As an alternate strategy for feeding on relatively small prey, some predators have evolved filter feeding mechanisms (6–8), but this high-drag foraging strategy is generally limited to slow and steady speeds and very large predator/prey size ratios >10^3 (7) where the size of the mouth counteracts the prey's maneuverability advantage. However, several medium-size rorqual species filter feed on small prey but can additionally target dense schools of forage fish, such as anchovies, sand lance, herring, and capelin at smaller predator/prey size ratios of 10^2 (9, 10). Fish of this size have the speed and maneuverability to quickly disperse if disturbed (Fig. 1*B* and Movie S1), and prior studies have found that prey are more likely to respond if approaching predators are large (11). The distance from the predator at which fish initiate an escape response (i.e., the reaction distance) is, thus, a critical factor in determining if an individual will escape an attack, and it follows that piscivorous filter feeding is only efficient for a large-bodied predator if it can attenuate the effectiveness of its prey's escape response; this study asks what mechanisms underlie a rapidly approaching whale's ability to avoid dispersing this potential energy source before it can be consumed.

Large filter feeding marine vertebrates that consume planktonic prey have evolved in several independent lineages of fishes and mammals (8) with most extant groups exhibiting slow and steady swimming speeds during foraging (7). In contrast, rorqual whales (a paraphyletic group within crown Balaenopteroidea) are unique in exhibiting a specialized lunge filter feeding strategy that is characterized by whole body acceleration and the intermittent and rapid engulfment of extremely large quantities of prey (6, 12). Among the largest animals of all time, rorquals range in size from 6 to 30 m, and all species exhibit at least part-time microphagy on krill (13) at a predator/prey length ratio on

Significance

Rorqual whales include the largest predators of all time, yet some species capture forage fish at speeds that barely exceed their quarry, suggesting that highly maneuverable fish should easily escape. We found that humpback whales delay the expansion of their jaws until very close to schools of anchovies, and it is only at this point that the prey react, when it is too late for a substantial portion of them to escape. This suggests that escape responses of these schooling fish, which have evolved under pressure from single-prey feeding predators for millions of years before the advent of lunge feeding, are not tuned sufficiently to respond to predators that can engulf entire schools, allowing humpback whales flexibility in prey choice.

Author contributions: D.E.C., N.C., P.D., and J.A.G. designed research; D.E.C., N.C., and P.D. performed research; D.E.C., N.C., P.D., and J.P. contributed new analytical tools; D.E.C., N.C., and P.D. analyzed data; J.A.G. administered the project and acquired funds; P.D. and J.A.G. supervised the project; P.D. and J.A.G. contributed substantially to manuscript drafts; and D.E.C. and N.C. wrote the paper.

The authors declare no competing interest.

This article is a PNAS Direct Submission.

Data deposition: The data reported in this paper have been deposited in the Stanford Digital Repository, https://purl.stanford.edu/mt574ws5287.

[1]To whom correspondence may be addressed. Email: davecade@stanford.edu.

[2]D.E.C. and N.C. contributed equally to this work.

[3]Present address: Scottish Association for Marine Science, Oban, Argyll PA37 1QA, United Kingdom.

This article contains supporting information online at https://www.pnas.org/lookup/suppl/doi:10.1073/pnas.1911099116/-/DCSupplemental.

First published December 23, 2019.

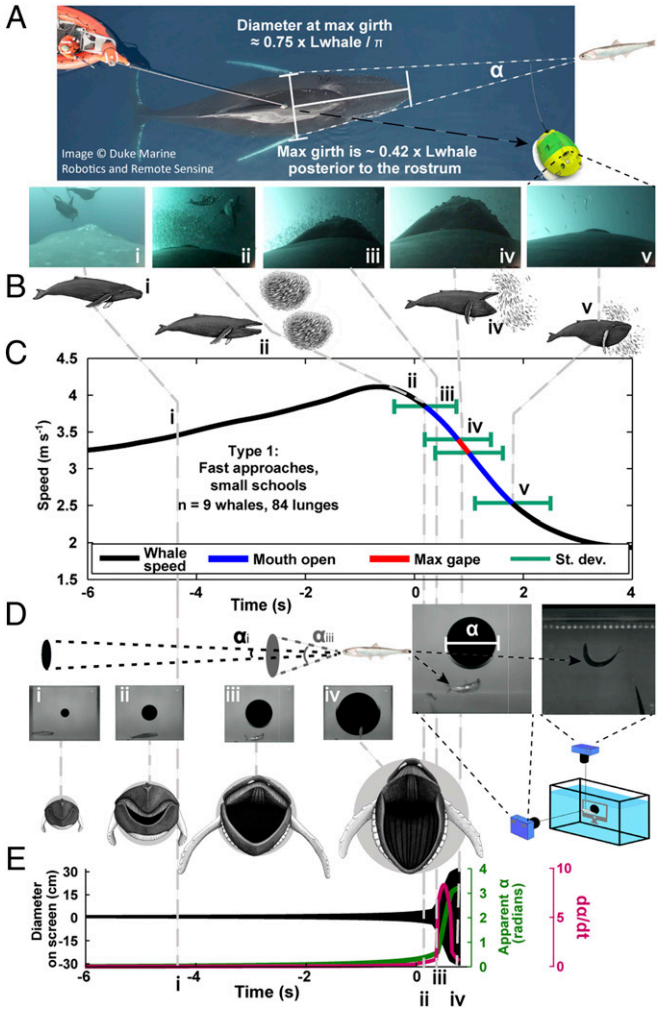

Fig. 1. This study combined field data, laboratory playbacks, and modeling. Points i–v are time aligned. (*A*) Suction cup video and 3D accelerometry tags were deployed on anchovy feeding (AF) humpback whales in California, USA. (*B*) Video recorded the behavior of schools as well as the timing of engulfment in relation to fish schools and to the whale's own acceleration profile. Fish did not break the school until the mouth opening (MO) event. (*C*) Mean speed profile of a Type 1 humpback whale. Lunge feeding is most efficient when engulfment coincides with deceleration. (*D*) Speed and engulfment were parameterized into looming stimuli and played back to anchovies in the laboratory. Anchovies demonstrated C-start escape responses at consistent thresholds of dα/dt. (*E*) Stimuli parameterized from predator data, as opposed to a constant approach speed, increased rapidly after the tips of the jaws were wider than the whale's maximum girth.

the order of 10^3. At these size differences, any prey maneuverability advantage is compensated for by the scale of the predator's mouth that would require prey to detect a threat from thousands of body lengths away and travel hundreds of body lengths per second to escape (2, 4). Indeed, when rorquals feed on krill, no escape response is observed (Movie S1). In contrast, some rorqual species hunt forage fish that are much more maneuverable than themselves and can actively escape (Movie S1), despite maximum lunge speeds that are the same or slower than for lunge feeding on krill (14). Hunting techniques that increase prey packing density, such as corralling and bubble netting have been noted in some rorqual species (15), but it has not been explained how an individual predator at this extreme body mass can, subsequently, accelerate toward a prey school without then dispersing the school.

Engulfment feeding on volumes of water that can exceed body mass is inherently an energetically costly endeavor (6, 16), and engulfment feeding on fish adds additional energetic costs as it commonly requires pursuit and aggregating maneuvers before engulfment. Additionally, while krill feeding (KF) whales use kinematically consistent and energetically efficient approach profiles, fish feeding whales use variable speeds and engulfment timings that can require higher energetic outputs since they involve continued body acceleration even after water starts to fill and expand the buccal cavity (14, 17). In this study, we sought to explain why fish feeding whales were less consistent in attack kinematics and posited that interactions between whales and maneuverable schooling prey played a role in modulating this behavior.

There is fossil evidence from freshwater deposits that schooling has existed as a fish behavior since, at least, 30–40 Ma earlier than when extreme gigantism arose in rorqual whales (18, 19). The transition to the age of giants was coincident with changes in oceanographic processes that encouraged upwelling and the formation of dense swarms of zooplankton (19). Although physical processes likely drive the aggregations of small-bodied plankton, forage fish aggregations are behaviorally mediated and likely evolved as a predator deterrent (20–22). It is, thus, likely that fish feeding whales benefit from the "rare enemy effect" (23) whereby the evolution of prey behavior, including the timing of their response to threats, has been driven by their more common encounters and long evolutionary history with predators that consume individual prey. We demonstrate how antipredator strategies related to schooling behaviors are, thus, counterproductive to avoiding large engulfment feeders.

Schooling in fish serves to intimidate or confuse predators targeting individual fish by either dissuading their attacks or making them less likely to succeed (5, 20–22). In contrast, a short-range flight response to a rapid predator approach manifests on an individual basis after a threshold of capture likelihood is passed. In both terrestrial and aquatic systems, there is pressure on individuals in an aggregation to not respond too early (24) as quick accelerations cannot only be energetically costly, jeopardizing future escape ability, but also leave the individual isolated from the group and much more vulnerable to predation (refs. 25 and 26 and Movie S1). The threshold of an observed predator approach at which prey respond is based on a combination of the size and speed of the predator (27–29). While fish can detect physical stimuli via the lateral line at very close proximity (~2 prey body lengths) (30, 31), fish in good visual conditions can detect approaching potential predators from much further away. Across taxa, potential prey have been shown to judge a potential predator's approach using some combination of the rate of change in the visual angle of a predator's outline (29, 32–34) and the apparent size of the approaching potential predator (27, 34–36). Escape responses of fish are, therefore, commonly investigated using visual looming stimuli to quantify the threshold at which escape decisions occur (Fig. 1 *D* and *E* and 27, 28, 33–38). Constant predator approach speeds are typically used to determine the specific range of looming thresholds (LTs) that stimulate escape responses (e.g., refs. 28, 34, and 38); in this study, we supplemented this technique by additionally exposing anchovies (*Engraulis mordax*) to looming stimuli directly parameterized on anchovy-feeding (AF) and KF humpback whale (*Megaptera novaeangliae*) speed and engulfment data collected from on-animal video biologging tags (14).

We used these looming stimulus experiments to determine the LTs at which individual anchovies responded to approaching predators in general, and humpback whales in particular. We subsequently collected additional field data from humpback whales attacking swimming schools of anchovies at high speed in Southern California (referred to throughout as Type 1 approaches) and contrasted those approaches with previously reported, relatively slow lunge feeding attacks (Type 2) on a relatively stationary

school of anchovies in Monterey Bay several times the size of the attacking whale (ref. 14 and Movie S2). We used mean data from both types of approaches and the experimentally derived LTs of anchovies to simulate how catch percentages would be affected by varying speed and engulfment profiles of the predator and calculated under what scenarios fish feeding whales would be incentivized to maximize catch percentage or, alternatively, to minimize the energetic cost of engulfment. Using this combination of field studies, laboratory experiments, and simulations (Fig. 1), we show how fish feeding humpback whales use not speed or maneuverability but stealth and deception (Fig. 2) to minimize and manipulate the escape responses of prey that have been evolving under pressure from particulate predators for millions of years before lunge feeding appeared as a strategy.

Results

Lunge Feeding Kinematics. The energetic costs of lunge feeding increase with increasing speed or if the whale accelerates against the increasing mass of engulfed water (Fig. 3). Therefore, lunge feeding involves biomechanically superfluous energetic costs if the onset of mouth opening (MO) does not coincide with peak speed: if MO is after peak speed, the whale uses energy to accelerate to higher speeds than necessary for engulfment, but if MO is before peak speed, the whale has to accelerate tons of engulfed water in addition to its own mass. Type 1, AF humpback whales (n = 9) reached maximum lunge speeds of 4.5 ± 0.8 m s^{-1} (mean ± SD) and were moving 3.8 ± 0.7 m s^{-1} at MO (95% confidence interval 0.5–1.0 m s^{-1} slower than peak) (Fig. 1*C*). MO varied considerably from peak speed (2.0 ± 2.4 s after) but was much more consistently related to a point of inflection in the speed profile before a period of rapid deceleration (0.2 ± 0.6 s after, *SI Appendix*, Fig. S3). In contrast, the Type 2 AF whale fed much more slowly (mean speed at engulfment: 2.2 ± 0.4 m s^{-1}, mean maximum speed: 2.5 ± 0.5 m s^{-1}), but also had highly variable MO times that averaged 1.1 ± 1.5 s before peak speed (Fig. 4*C*). Therefore, neither scenario displayed the cost-effective strategies of KF whales where engulfment initiation and peak speed coincide (14), implying that AF involves additional energetic costs.

Escape Responses of Anchovies. The perception of an approaching predator by a small fish can be represented as the angle (α) of the predator's maximum profile subtended on the retina of the prey (Fig. 1 *A* and *D*), and fish respond to the stimulus when the rate of change (dα/dt) of α crosses a species-specific threshold (32, 33) that may be modulated by the size of the stimulus (27, 34, 35). Using high-speed cameras, we recorded individual anchovies initiating escape responses to the constant speed approach of an expanding disk (Fig. 1*D* and Movie S3) at 1.66 ± 0.37 (range: 0.89–2.06 rad s^{-1}), a range that spanned 18 animation frames (300 ms). Other formulations of the response parameter that take into account both α and dα/dt were also calculated but did not better describe the observed variation in fish responses (see *SI Appendix*, Fig. S4 for a full discussion), so results presented here are for the simplest response model (a threshold of dα/dt) that retains high explanatory power. Since the stimulus response is triggered by the sensory system a few milliseconds before the fish makes a visible reaction (28), the range reported (referred to throughout as LT_{exp}) is the "true" LT after accounting for an estimated visual response latency of 61 ms. The visual response latency (range of 33–88 ms) was determined in separate experiments from the timing of anchovy escape responses to a bright flash and were comparable to visually mediated responses in other fish species (28, 37).

To determine how fish responded to actual predator approaches, we parameterized looming stimuli directly from KF and AF humpback whale speed and engulfment data (14) applied to a 10.5 m humpback whale (Fig. 1). Because the maximum diameter of the whale is located >4 m from its rostrum, in both the AF and the KF approaches, α increased slowly until a critical point during MO when the apparent angle of the jaw exceeded the apparent angle of the whale's maximum girth. At this apparent mouth opening (AMO) point, the widest part of the predator was instantaneously closer to the fish, was approaching near maximum speed, and was itself rapidly expanding as the whale's mouth approached maximum gape. All three of these factors combined to cause a rapid increase in α and a corresponding abrupt increase in dα/dt that encompassed the entire LT_{exp} range within a single animation frame (<17 ms) in both AF and KF playbacks (Fig. 1*E*, *SI Appendix*, Figs. S5 and S7, and Movie S3). Individual anchovies initiated escape between 30 and 270 ms after AMO (*SI Appendix*, Table S1 and Fig. S5) with responses to the AF playback (140 ± 80 ms after) not significantly different (P = 0.56) from responses to the KF playback (120 ± 80 ms after), implying that responses to KF and AF playbacks could not be further differentiated. Many of the escape responses occurred within the calculated visual latency range, but some were delayed up to an additional 180 ms (*SI Appendix*, Table S1), suggesting that for

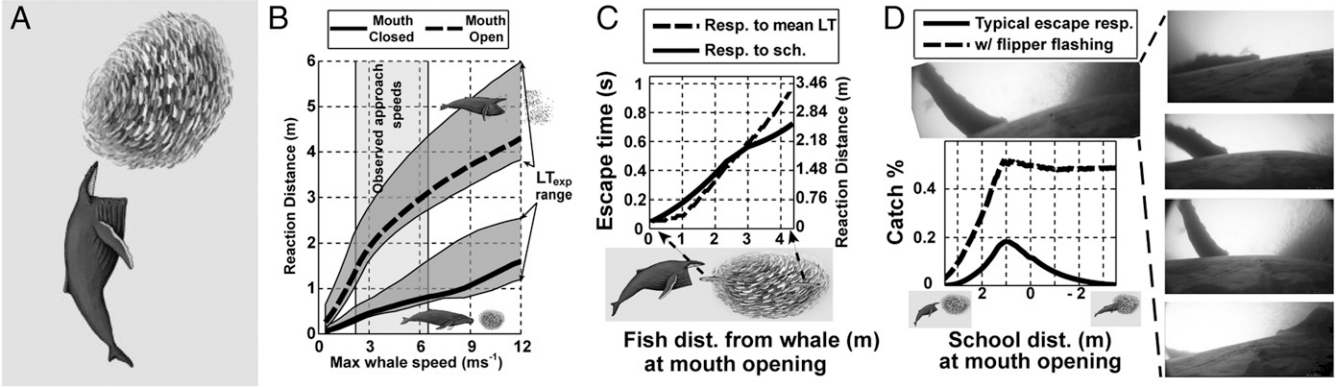

Fig. 2. Anchovies are evolutionarily conditioned to avoid small, fast, and mobile particulate feeding predators by forming and reacting as dense schools. Humpback whales, as less commonly encountered predators, take advantage of this strategy in 4 ways: (*A*) Lunge filter feeding enables engulfment of many individuals simultaneously. (*B*) MO close to the school results in shorter prey reaction distances equivalent to the whale's distance at apparent MO (AMO). This value will be intermediate between the 2 extremes of theoretical approaches (mouth always open and mouth always closed). (*C*) Anchovies at the back of a fleeing school will respond directly to the fish fleeing around it, however, these fish have less time to respond (resulting in a shorter reaction distance) than if they could see the approaching predator directly. (*D*) Humpback whale flippers can be 3 to 4 m in length—although not themselves used as weapons, they have white undersides that can be used to scare escaping fish back toward the school (see also Fig. 4 and Movie S4).

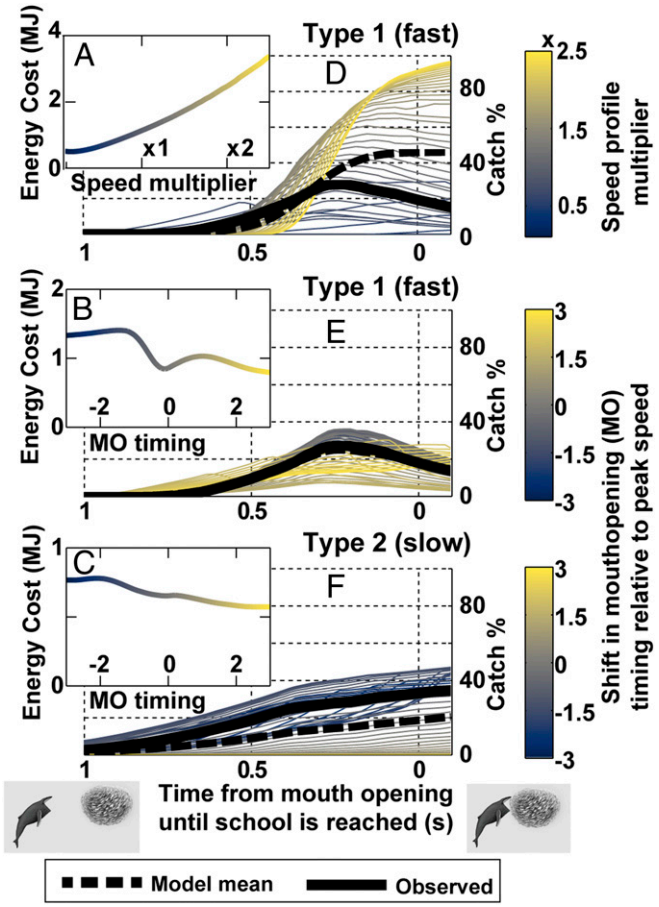

Fig. 3. Energy use during lunge feeding is a product of speed and engulfment timing, while catch percentage is a product of kinematics and the timing of engulfment with respect to the school. (*A*) Energy cost as speed of the mean fast humpback approach is varied. (*B*) Cost as the timing of MO relative to peak speed of the fast approach is varied. (*C*) Cost of varying MO timing for a slow approach. (*D–F*) How catch percentage varies both as a function of school distance at MO and with variation in speed (*D*) or MO timing (*E* and *F*). Thick black lines highlight the mean observed approaches.

some fish the abrupt increase in the stimulus at AMO may have been an unfamiliar threat requiring additional neural processing before the escape response was initiated. Crucially, a narrow temporal window around AMO of 34 ms spanned a dα/dt range (AF: 0.23–2.33, KF: 0.20–4.24 rad s^{-1}) that encompassed the entire range of true LT_{exp} and additionally maximized alternative response model forms that incorporated both α and dα/dt (*SI Appendix*, Fig. S4). The implication is that all fish, regardless of variation in response latency, respond very shortly after AMO. In 80 on-animal video observations of whale attacks on anchovy schools in situ, 67 showed the school dispersing closely following the observed MO (mean: 300 ± 360 ms after) with the earliest observed school dispersion occurring 400 ms before MO.

Video of whales approaching without opening their mouths (e.g., Movie S4) demonstrate that fish maintain school cohesion as the whale approaches, confirming our observation that the rapid expansion of the looming stimulus at AMO is likely responsible for initiating the anchovy escape response. If a whale, at typically observed attack speeds of ∼2–7 m s^{-1}, approaches without opening its mouth, it would be able to get within 1 m of the school before triggering a response (Fig. 2*B*). The substantial distance of the widest part of the (large) predator from the actual threat (the jaws) (Fig. 1*A*) serves to mask the distance of the approach until the jaws extend beyond the apparent profile and engulfment has already begun. The fundamental consequences of this are 1) delaying MO to be close to the school masks the threat of predation, and 2) faster approach speeds have a smaller effect on anchovy responses than does MO timing (Fig. 2), implying that faster approach speeds could increase capture rates since whales can better overcome prey escapes without startling their prey earlier.

Prey Capture Effectiveness under Different Engulfment Scenarios. We calculated when each individual fish in a school would escape from an approaching whale under different scenarios, assuming that fish would initiate escape responses at minimum, mean, or maximum LT_{exp} + 61 ms (a "quick response" using the estimated visual response latency) or + 261 ms (a "slow response" representative of the observed variation in response to AMO). Our models assume a visual stimulus since fish can likely perceive threats from a much further distance using vision than if relying on physical stimulus detection. That is, while there are no published data regarding the lateral line predator detection distance of schooling fish, adult fish, or any fish responding to a wave created from a whale-sized approaching object, our assumption that this distance is short is supported by previous research which has found that 1) lateral line detection of approaching predators in larval fish is <1.5 cm [1 to 2 prey body lengths (30, 31)], 2) lateral line detection of prey and neighboring fish is also 1 to 2 body lengths (39, 40), 3) the lateral lines of fish in motion are more than 3 orders of magnitude less sensitive than still fish (41), and 4) the lateral line in schooling fish is actively engaged in maintaining the school (42). Accordingly,

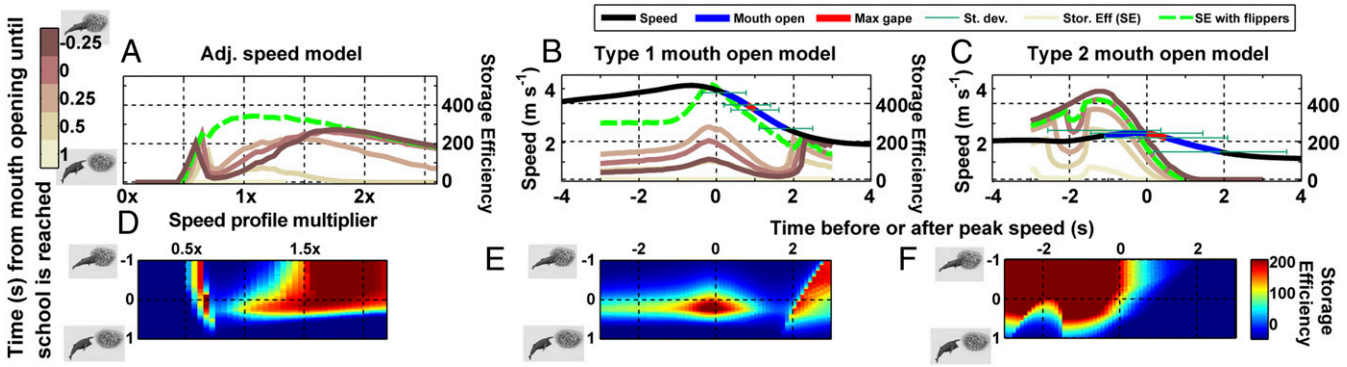

Fig. 4. Efficiency is affected by catch percentage and energy use as shown in Fig. 3. (*A*) At high speeds, efficiency drops sharply if whales open their mouths too early. Efficiency is increased for moderate speeds when the flippers are used to scare early fleeing fish back toward the mouth. (*B*) The timing of the MO in relation to the school has a much greater effect on efficiency than the timing in relation to peak speed. (*C*) At slow speeds, the timing of engulfment is less critical as efficiency can remain high.

results and discussion focus on simulations where the school is visually stimulated to respond at or before the whale reaches the school. Fish in the center of a school that cannot see the approaching whale directly do use the lateral line (in addition to vision) to initiate escape when others escape around them (40, 42); however, due to the time it takes a wave of response to pass through the school (*SI Appendix*), fish >2 m from the edge of the school actually have less time to escape than if they had been able to directly observe the oncoming predator (Fig. 2*C*).

For all simulations, we used a representative fish length of 12 cm and a school packing density of (1 body length)^3 per fish (*SI Appendix*) and assumed that the school was bigger than the engulfment volume of the whale. As predicted, prey capture is maximized when the whale begins MO close to the edge of the school (Fig. 3) and increases as the predator increases its speed (Fig. 3*A*). The cost of mistiming this event, however, is prodigious; in all scenarios, if the whale's mouth opens 1 s before reaching the school, the LT_{exp} is exceeded at a distance that allows every fish to escape. The increasing steepness of the slopes of the curves with speed (Fig. 3*A*) also demonstrates how precise timing becomes more important as speed increases. At slow speeds (Fig. 3*C* and *SI Appendix*, Fig. S1), catch percentage is maintained at ∼40% for a wide range of engulfment timings and does not increase substantially even in models with slow fish responses (*SI Appendix*, Fig. S1). In contrast, at faster speeds, if precise engulfment timing is obtained, the opportunity to catch more fish roughly doubles when fish are modeled to respond more slowly. Humpback whales also have a built-in buffer against early-responding fish; they are unique among cetaceans in having extraordinarily long flippers (∼30% of body length, see *SI Appendix*) with white undersides that they have been observed to rotate and extend during engulfment (ref. 43, Fig. 2*D*, and Movie S4) to expose fleeing prey to an additional stimulus that serves to turn fish back toward the school, increasing catch; this effect was most pronounced in models that assumed faster responses and faster speeds (*SI Appendix*, Fig. S2).

Foraging Efficiency. To examine how energetically efficient lunge feeding must balance energy intake (E_{in}) against locomotor costs (E_{out}, calculated from first principles; ref. 44), we defined the foraging efficiency as the *surplus efficiency*: the net energy gain from fish that would be captured proportional to the energy that would be spent: $(E_{in} - E_{out})/E_{out}$. Type 1 approaches, with more kinematic consistency, were used as a model to vary approach speed (which affected both E_{out} and E_{in}), and both approach types were used to model how distance from the school at MO (affecting E_{in}) and engulfment timing (affecting both E_{out} and E_{in}) influenced overall energetic gain.

A whale approaching a school using the Type 2 speed profile would use 68% more energy by doubling its speed and 275% more energy by quadrupling its speed. Energetic cost is minimal when MO is at peak speed or later (Fig. 3*A*) and maximal when the mouth is opened 1 to 2 s before peak speed as the whale must accelerate against increased drag from engulfment (Fig. 3 *B* and *C*). Accordingly, efficiency for the fast scenario peaked when the mouth opened coincident with engulfment and when the mouth opened exactly when the humpback reached the fish school (Fig. 4 *B* and *E*). Critically, particularly in faster scenarios if the whale mistimes its lunge in relation to the fish school, its efficiency drops more quickly than if it mistimes its engulfment in relation to acceleration (Fig. 4*E*). For example, if an approaching whale using a Type 1 profile opens its mouth 0.25 s before the fish school is reached, its efficiency would drop by 36%, but if it opens its mouth 0.25 s before peak speed, its efficiency drops by only 11%.

Comparisons with Other Predators. The attack model used to determine α and dα/dt at every point of approach (44) can also be parameterized with size and speed data from other predators. For an AF particulate predator, the California sea lion (*Zalophus californianus*), the mean LT_{exp} for an anchovy would be exceeded by ∼0.5 m before the fish is reached (*SI Appendix*, Fig. S7), allowing it to escape a distance (6.6 cm) that is greater than the width of a sea lion jaw (*SI Appendix*) and implying that the sea lion (predator/prey size ratio ∼10^1) must rely on its noted maneuverability (45) to be successful. When the stimulus is parameterized with blue whale size and attack data, similar to humpback whales, mean LT_{exp} is not reached until AMO. Due to the long engulfment duration of blue whales (14), however, AMO is still 1.2 s and 2.8 m before the mouth even finishes opening. Due to the consequent increased time to escape, <15% of fish would be caught (*SI Appendix*, Fig. S7*B*), potentially explaining why blue whales are known to be almost exclusively euphausivores (13).

In prior experiments with other species, it has been suggested that an individual's response to a specific LT is progressively inhibited at larger stimulus sizes (27, 34, 35). That is, individuals would be less likely to respond at the same values of dα/dt if the object is closer, or, as in this unique case, substantially larger. This would imply that humpback whales have an inherent advantage over smaller predators: At any given distance from the prey, they would appear much larger than a smaller predator, and, at any given α, α will be increasing more slowly since the whale would be further away. Applying a response model that incorporates α inhibition (η in ref. 35, see *SI Appendix*, Fig. S4) results in an increased catch of 30% above the dα/dt threshold model in Type 1 approaches and no increase in Type 2 approaches (*SI Appendix*, Fig. S1).

Discussion

For predator/prey size ratios of 10^0–10^1, the speed of a predator can overcome the maneuverability of prey when $v > \sqrt{r}$, where v is the ratio of predator speed to prey speed and r is the ratio of turning radii (a measure of maneuverability) (2–4). At predator/prey size ratios of 10^2, the size ratio of humpbacks feeding on fish, r is also 10^2, and a predator would have to be more than 10 times as fast as its prey to overcome its maneuverability disadvantage. In contrast, we observed that the average humpback whale speed at MO of 3.8 m s^{-1} [with even slower attack speeds also reported (14, 46)] was only 60% higher than mean anchovy escape speeds (*SI Appendix*, Fig. S6) and decreased rapidly throughout the lunge, implying that these predators should not theoretically be able to capture fish.

If a group of small fish is treated as a unit, however, the predator/prey size ratio for humpback whales and anchovy schools is decreased to 10^1. Humpback whales in this study pursuing anchovies in concert with common dolphins (Movie S2) sustained speeds of up to 6 m s^{-1} for up to a minute before slowing down on the final approach to a lunge. The speed of an anchovy school is likely no greater than an individual anchovy's maximum sustained swimming speed of 60 cm s^{-1} (47)—about 10 times slower than the observed humpback whale speeds—implying that, on approach, these whales overcome the $v = \sqrt{r}$ restriction and providing an additional rationale for high speeds of attack despite the increased precision in engulfment timing required. Once an imminent, individual threat is perceived by the prey, however, an individual prey escape response is initiated whereby burst speeds combined with individual maneuverability become the dominant escape mechanisms and the school disperses. Anchovies have the performance capabilities to evade capture if they respond to a threat with sufficient time; our simulations suggest that, if the LT of response was reduced (i.e., anchovies were more sensitive to threats) to 0.5 rad s^{-1}, 97% of fish would escape since they would begin to flee

earlier, and if LT was reduced to 0.3 rad s^{-1}, 99.8% of fish would escape. These results explain how whales catch fish despite the capabilities of their prey to escape by delaying the moment at which individual fish perceive the threat. It should additionally be noted that the initiation of individual escape responses in situ may be further delayed from what we found in the laboratory since, in natural settings, existence within a large group often inhibits individual flight responses due to the risk dilution effect in concert with direct occlusion of the stimulus (34, 48). This conserved behavioral feature is safer for an individual when it is targeted by predators hunting single fish but is counterproductive when the school itself is in danger of predation and, as such, may further serve to increase the captured proportion of a school, resulting in catches closer to the slow response scenarios (*SI Appendix*, Figs. S1 and S2).

We found that efficiency is dominated more by catch percentage than by the energetic cost of a lunge (Fig. 4). Therefore, the most important factor that will increase foraging efficiency in engulfment filter feeders is the maintenance of packing density within the school. Small prey, such as krill and copepods, form large aggregations generally through passive processes, such as advection (49). Forage fish, in contrast, form schools actively and often explicitly as antipredation strategies (20–22). Humpback whales in many populations worldwide utilize a variety of strategies for inducing schooling fish into tighter aggregations including foraging in concert with particulate feeding predators (50) or by physically (15) or acoustically (51, 52) manipulating prey into tighter aggregations. The humpback whales in this study foraged by following common dolphins (*Delphinus sp.*) that herd fish into tighter schools or in concert with groups of California sea lions (Movie S2). However, these schools scattered into smaller highly maneuverable units during engulfment events (Movie S1), implying that the success of humpback whale foraging depends on delaying this scattering response. Our results support this analysis whereby whales use their bulk to hide in plain sight: Even though they are visible to individual anchovies on the outside of a school, they do not appear to be a threat since their visual approach profile does not reach anchovies' LT before they open their mouths and begin engulfment, at which point it is too late for a substantial portion to disperse. The paradoxical increased risk to individuals that results from staying with the school instead of dispersing early likely results from forage fish fine-tuning visual response thresholds over evolutionary timescales for particulate feeding predators—a threat for which it is safer for each individual to stay in the school (26). This strategy, however, is not effective for avoiding predation by a lunge feeding whale of extreme size that can engulf a large portion of a school simultaneously.

Schools of anchovies are highly mobile, and, consequently, the overall feeding rates we observed were substantially lower (3.9 ± 2.0 lunges h^{-1}) than for California KF whales (23.0 ± 17.9 lunges h^{-1}). Over long timescales, it is, thus, only efficient to forage on fish if the energy intake from individual feeding events is higher than for KF events. Indeed, we found that an AF whale catching 40% of a school would get 6.8 times more energy per lunge than a KF whale (see the details in the *SI Appendix*). Additionally, the locomotor cost of AF is also higher than for KF. Likely because prey escape is a minimal consideration during KF (e.g., Movie S1), these whales appear to adopt the most hydrodynamically efficient engulfment profiles where MO coincides with maximum speed (14). In contrast, AF humpback whales, which, like other animals that perform banking turns (53), can use their flippers to increase maneuverability at higher speeds (54) and make fine-scale adjustments in attack speed and body orientation that facilitate the onset of engulfment as close as possible to the fish school, even if that means accelerating against the drag of an open mouth (Fig. 4). The surprisingly energetically costly engulfment profiles previously noted for fish feeding whales (14, 17) can, thus, be explained by the need to time engulfment to be proximal to the fish school, thereby maximizing energy intake (Fig. 4).

High-speed engulfment filter feeding by large predators is a relatively recent evolutionary phenomenon; it is likely that rorqual whales evolved this feeding modality from an ancestral raptorial suction feeding state to take advantage of upwelling-induced zooplankton patchiness that appears to have become more readily available in the late Miocene (19). Forage fish, such as anchovies, however, have likely been under attack from a variety of single-prey feeding predators for hundreds of millions of years. In contrast to larger baleen whale species that specialize on zooplankton, we suggest that the large size of humpback whales has allowed them to exapt their unique lunge filter feeding mechanism to exploit some aspects of the antipredator defenses of anchovies, allowing them to feed on a greater variety of prey. Consequently, the enhanced foraging flexibility resulting from this generalist strategy has likely contributed to the humpback whale's ability to recover from 20th century near extermination (55) and might continue to make them less vulnerable to future climatic-induced ecosystem changes than more specialist and more endangered ocean giants (56).

Data Availability. R and Matlab code to calculate the diameter of the looming stimulus and the energetic cost of a lunge is available at https://purl.stanford.edu/mt574ws5287 (44).

ACKNOWLEDGMENTS. Special thanks to John Calambokidis, Ari Friedlaender, and David Johnston and the crew of the Research Vessel Truth for spearheading field operations; to Jo Welsh for anchovy specimens; to Madison Bashford, Ben Burford, and Diana Li for experimental assistance; to Jake Linsky for analytical assistance; to Jessica Bender for sea lion illustrations; and to Alex Boersma for the remainder of the illustrations. Thanks should be extended to the three anonymous reviewers whose careful considerations strengthened the manuscript. This work was funded with NSF Integrative Organismal Systems Grant 1656691, Office of Naval Research Young Investigator Program Grant N000141612477, and Stanford University's Terman and Bass Fellowships. All procedures were conducted under institutional Institutional Animal Care and Use Committee guidelines and National Marine Fisheries Service permit 16111.

1. R. P. Wilson *et al.*, Mass enhances speed but diminishes turn capacity in terrestrial pursuit predators. *eLife* **4**, e06487 (2015).
2. P. Domenici, The scaling of locomotor performance in predator-prey encounters: From fish to killer whales. *Comp. Biochem. Physiol. A Mol. Integr. Physiol.* **131**, 169–182 (2001).
3. H. C. Howland, Optimal strategies for predator avoidance: The relative importance of speed and manoeuvrability. *J. Theor. Biol.* **47**, 333–350 (1974).
4. P. W. Webb, V. De Buffrénil, Locomotion in the biology of large aquatic vertebrates. *Trans. Am. Fish. Soc.* **119**, 629–641 (1990).
5. P. Domenici *et al.*, How sailfish use their bills to capture schooling prey. *Proc. R. Soc. B: Biol. Sci.* **281**, 20140444 (2014).
6. J. A. Goldbogen *et al.*, How baleen whales feed: The biomechanics of engulfment and filtration. *Annu. Rev. Mar. Sci.* **9**, 367–386 (2017).
7. M. Simon, M. Johnson, P. Tyack, P. T. Madsen, Behaviour and kinematics of continuous ram filtration in bowhead whales (Balaena mysticetus). *Proc. R.Soc.B. Biol. Sci.* **276**, 3819–3828 (2009).
8. M. Friedman *et al.*, 100-million-year dynasty of giant planktivorous bony fishes in the Mesozoic seas. *Science* **327**, 990–993 (2010).
9. A. H. Fleming, C. T. Clark, J. Calambokidis, J. Barlow, Humpback whale diets respond to variance in ocean climate and ecosystem conditions in the California current. *Glob. Change Biol.* **22**, 1214–1224 (2016).
10. D. L. Wright, B. Witteveen, K. Wynne, L. Horstmann-Dehn, Evidence of two subaggregations of humpback whales on the Kodiak, Alaska, feeding ground revealed from stable isotope analysis. *Mar. Mamm. Sci.* **31**, 1378–1400 (2015).
11. W. E. Cooper, Jr, T. Stankowich, Prey or predator? Body size of an approaching animal affects decisions to attack or escape. *Behav. Ecol.* **21**, 1278–1284 (2010).
12. P. Brodie, Cetacean energetics, an overview of intraspecific size variation. *Ecology* **56**, 152–161 (1975).
13. A. Kawamura, A review of food of balaenopterid whales. *Sci. Rep. Whales Res. Inst.* **32**, 155–197 (1980).
14. D. E. Cade, A. S. Friedlaender, J. Calambokidis, J. A. Goldbogen, Kinematic diversity in rorqual whale feeding mechanisms. *Curr. Biol.* **26**, 2617–2624 (2016).
15. D. Wiley *et al.*, Underwater components of humpback whale bubble-net feeding behavior. *Behaviour* **148**, 575–602 (2011).
16. A. Acevedo-Gutiérrez, D. A. Croll, B. R. Tershy, High feeding costs limit dive time in the largest whales. *J. Exp. Biol.* **205**, 1747–1753 (2002).

17. M. Simon, M. Johnson, P. T. Madsen, Keeping momentum with a mouthful of water: Behavior and kinematics of humpback whale lunge feeding. *J. Exp. Biol.* **215**, 3786–3798 (2012).
18. N. Mizumoto, S. Miyata, S. C. Pratt, Inferring collective behaviour from a fossilized fish shoal. *Proc. Biol. Sci.* **286**, 20190891 (2019).
19. G. J. Slater, J. A. Goldbogen, N. D. Pyenson, Independent evolution of baleen whale gigantism linked to Plio-Pleistocene ocean dynamics. *Proc. Biol. Sci.* **284**, 20170546 (2017).
20. J. Krause, G. D. Ruxton, *Living in Groups* (Oxford University Press, 2002).
21. J.-G. J. Godin, Antipredator function of shoaling in teleost fishes: A selective review. *Nat. Can.* **113**, 241–250 (1986).
22. A. E. Magurran, The adaptive significance of schooling as an anti-predator defence in fish. *Ann. Zool. Fenn.* **27**, 51–66 (1990).
23. R. Dawkins, *The Extended Phenotype: The Gene as the Unit of Selection* (Freeman, ed. 1982, 1982).
24. R. C. Ydenberg, L. M. Dill, The economics of fleeing from predators. *Adv. Study Behav.* **16**, 229–249 (1986).
25. A. E. Magurran, T. J. Pitcher, Provenance, shoal size and the sociobiology of predator-evasion behaviour in minnow shoals. *Proc. R. Soc. Lond. B Biol. Sci.* **229**, 439–465 (1987).
26. C. C. Ioannou, F. Rocque, J. E. Herbert-Read, C. Duffield, J. A. Firth, Predators attacking virtual prey reveal the costs and benefits of leadership. *Proc. Natl. Acad. Sci.* **116**, 8925–8930 (2019).
27. N. Hatsopoulos, F. Gabbiani, G. Laurent, Elementary computation of object approach by wide-field visual neuron. *Science* **270**, 1000–1003 (1995).
28. A. Paglianti, P. Domenici, The effect of size on the timing of visually mediated escape behaviour in staghorn sculpin *Leptocottus armatus*. *J. Fish Biol.* **68**, 1177–1191 (2006).
29. P. W. Webb, Avoidance responses of fathead minnow to strikes by four teleost predators. *J. Comp. Physiol.* **147**, 371–378 (1982).
30. W. J. Stewart, G. S. Cardenas, M. J. McHenry, Zebrafish larvae evade predators by sensing water flow. *J. Exp. Biol.* **216**, 388–398 (2013).
31. M. J. McHenry, K. E. Feitl, J. A. Strother, W. J. Van Trump, Larval zebrafish rapidly sense the water flow of a predator's strike. *Biol. Lett.* **5**, 477–479 (2009).
32. P. Domenici, The visually mediated escape response in fish: Predicting prey responsiveness and the locomotor behaviour of predators and prey. *Mar. Freshwat. Behav. Physiol.* **35**, 87–110 (2002).
33. L. M. Dill, The escape response of the zebra danio (Brachydanio rerio) I. The stimulus for escape. *Anim. Behav.* **22**, 711–722 (1974).
34. A. M. Hein, M. A. Gil, C. R. Twomey, I. D. Couzin, S. A. Levin, Conserved behavioral circuits govern high-speed decision-making in wild fish shoals. *Proc. Natl. Acad. Sci. U.S.A.* **115**, 12224–12228 (2018).
35. T. Preuss, P. E. Osei-Bonsu, S. A. Weiss, C. Wang, D. S. Faber, Neural representation of object approach in a decision-making motor circuit. *J. Neurosci.* **26**, 3454–3464 (2006).
36. I. Temizer, J. C. Donovan, H. Baier, J. L. Semmelhack, A visual pathway for looming-evoked escape in larval zebrafish. *Curr. Biol.* **25**, 1823–1834 (2015).
37. R. Batty, Escape responses of herring larvae to visual stimuli. *J. Mar. Biol. Assoc. U. K.* **69**, 647–654 (1989).
38. C. K. Faulk, L. A. Fuiman, P. Thomas, Parental exposure to ortho, para-dichlorodiphenyltrichloroethane impairs survival skills of Atlantic croaker (*Micropogonias undulatus*) larvae. *Environ. Toxicol. Chem.* **18**, 254–262 (1999).
39. J. Montgomery, R. Milton, Use of the lateral line for feeding in the torrentfish (Cheimarrichthys fosteri). *N. Z. J. Zool.* **20**, 121–125 (1993).
40. E. J. Denton, J. Gray, Mechanical factors in the excitation of clupeid lateral lines. *Proc. R. Soc. Lond. B Biol. Sci.* **218**, 1–26 (1983).
41. I. Russell, B. Roberts, Active reduction of lateral-line sensitivity in swimming dogfish. *J. Comp. Physiol.***94**, 7–15 (1974).
42. K. Faucher, E. Parmentier, C. Becco, N. Vandewalle, P. Vandewalle, Fish lateral system is required for accurate control of shoaling behaviour. *Anim. Behav.* **79**, 679–687 (2010).
43. M. M. Kosma, A. J. Werth, A. R. Szabo, J. M. Straley, Pectoral herding: An innovative tactic for humpback whale foraging. *R. Soc. Open Sci.* **6**, 191104 (2019).
44. D. E. Cade, N. Carey, P. Domenici, J. Potvin, J. A. Goldbogen, Predator-informed looming stimulus experiments reveal how large filter feeding whales capture highly maneuverable forage fish. Stanford Digital Repository. https://purl.stanford.edu/mt574ws5287. Deposited 11 October 2019.
45. F. E. Fish, J. Hurley, D. P. Costa, Maneuverability by the sea lion *Zalophus californianus*: Turning performance of an unstable body design. *J. Exp. Biol.* **206**, 667–674 (2003).
46. A. J. Werth, M. M. Kosma, E. M. Chenoweth, J. M. Straley, New views of humpback whale flow dynamics and oral morphology during prey engulfment. *Mar. Mamm. Sci.* **35**, 1556–1578 (2019).
47. A. James, T. Probyn, The relationship between respiration rate, swimming speed and feeding behaviour in the Cape anchovy *Engraulis capensis* Gilchrist. *J. Exp. Mar. Biol. Ecol.* **131**, 81–100 (1989).
48. M. A. Gil, A. M. Hein, Social interactions among grazing reef fish drive material flux in a coral reef ecosystem. *Proc. Natl. Acad. Sci. U.S.A.* **114**, 4703–4708 (2017).
49. D. Lavoie, Y. Simard, F. J. Saucier, Aggregation and dispersion of krill at channel heads and shelf edges: The dynamics in the Saguenay-St. Lawrence marine park. *Can. J. Fish. Aquat. Sci.* **57**, 1853–1869 (2000).
50. E. Jourdain, D. Vongraven, Humpback whale (*Megaptera novaeangliae*) and killer whale (*Orcinus orca*) feeding aggregations for foraging on herring (*Clupea harengus*) in Northern Norway. *Mamm. Biol.* **86**, 27–32 (2017).
51. M. E. Fournet, C. M. Gabriele, F. Sharpe, J. M. Straley, A. Szabo, Feeding calls produced by solitary humpback whales. *Mar. Mamm. Sci.* **34**, 851–865 (2018).
52. T. Leighton, D. Finfer, E. Grover, P. White, An acoustical hypothesis for the spiral bubble nets of humpback whales, and the implications for whale feeding. *Acoust. Bull.* **32**, 17–21 (2007).
53. R. Mills, H. Hildenbrandt, G. K. Taylor, C. K. Hemelrijk, Physics-based simulations of aerial attacks by peregrine falcons reveal that stooping at high speed maximizes catch success against agile prey. *PLOS Comput. Biol.* **14**, e1006044 (2018).
54. P. S. Segre *et al*., Hydrodynamic properties of fin whale flippers predict maximum rolling performance. *J. Exp. Biol.* **219**, 3315–3320 (2016).
55. M. Bejder, D. W. Johnston, J. Smith, A. Friedlaender, L. Bejder, Embracing conservation success of recovering humpback whale populations: Evaluating the case for downlisting their conservation status in Australia. *Mar. Policy* **66**, 137–141 (2016).
56. V. J. D. Tulloch, É. E. Plagányi, C. Brown, A. J. Richardson, R. Matear, Future recovery of baleen whales is imperiled by climate change. *Glob. Change Biol.*, 10.1111/gcb.14573 (2019).

PNAS
www.pnas.org

Supplementary Information for

Predator-informed looming stimulus experiments reveal how large filter feeding whales capture highly maneuverable forage fish

David E. Cade
Nicholas Carey
Paolo Domenici
Jean Potvin
Jeremy A. Goldbogen

Corresponding author:
Email: davecade@stanford.edu

This PDF file includes:

Other supplementary materials for this manuscript include the following:

www.pnas.org/cgi/doi/10.1073/pnas.1911099116

Supplementary Information Text

List of abbreviations

α:	The apparent angle of an approaching predator or stimulus subtended on the retina of the prey
AF:	Anchovy-feeding
AMO:	Apparent Mouth Opening
CATS:	Customized Animal Tracking Solutions
dα/dt:	The change in the size of the looming stimulus over time (aka the loom rate)
E_{in}:	Energy from food (input)
E_{out}:	Energy expended (output)
HF:	High frequency
IACUC:	Institutional Animal Care and Use Committee
KF:	Krill-feeding
LT:	Looming Threshold
LT_{exp}:	experimentally determined Looming Threshold of response (in rad s^{-1})
MC:	Mouth Closing
MO:	Mouth Opening
SD:	Standard deviation
SE:	Surplus efficiency
SI:	Supplemental Information
SoCal:	Southern California study region
UAV:	Unoccupied Aerial Vehicle
U_{pred}:	Speed (of a predator)

Materials and Methods

This work used a combination of field data, laboratory experiments and modeling to describe the predator/prey interactions of humpback whales and anchovies. We first used mean published data on anchovy-feeding (AF) and krill-feeding (KF) humpback whales from (2) to parameterize laboratory looming threshold experiments with individual anchovies in the lab (see below). After determining the timing of anchovy escape responses to virtually approaching whales, we used new field data and the results of the laboratory experiments to test how predator speed, the timing of engulfment in relation to acceleration, and the timing of mouth opening in relation to a prey school affected how many fish a humpback whale could catch, and how much energy it spent doing so. We divided humpback whale attacks into two categories: Type 1 was the mean of new data from fast attacking whales tagged in Southern California (SoCal) feeding on mobile patches of anchovies ~1-2 m across; Type 2 was the mean of a previously published, slow-attacking whale from Monterey Bay, California (2) feeding on an anchovy school several times larger than its own size.

Field data collection and analysis

The humpback whale approach speeds used to create the looming stimuli in the lab experiments were averaged speed profiles derived from the krill-feeding and anchovy-

feeding humpback whales in (2). Data from additional humpback whales used for escape simulations were collected in August 2017 near Santa Barbara, California using suction-cup attached video and movement sensing tags from Customized Animal Tracking Solutions (CATS) (2, 3). All tags were deployed from a 6 m rigid-hull inflatable boat using a 6 m pole (Fig. 1a) under National Marine Fisheries Service permits 16111 as well as institutional IACUC protocols. Accelerometers were sampled at 400 Hz, magnetometers and gyroscopes at 50 Hz and, pressure, light, temperature and GPS at 10 Hz. All data were decimated to 10 Hz, tag orientation on the animal was corrected for, and animal orientation was calculated using custom-written Matlab scripts (following 2, 4). Animal speed for all deployments was determined using the amplitude of tag vibrations (5).

Engulfment timing from on-animal videos of humpback whales attacking anchovies was determined from the first indication of head rise and the last indication of the head falling (2). School dispersion happened over a range of times and parts of the targeted schools were blocked from view by the whale's body. Thus, it was not possible to determine the timing of the first fish to flee, however a time of school dispersion was estimated from the first time at least 50% of the visible school was observed to be scattering.

Fish Husbandry

All anchovies (*Engraulis mordax*) came from a stock of approximately 400 individuals kept at Hopkins Marine Station, Pacific Grove, CA, USA, in a 3200 L circular tank (2.5 m diameter, 0.65 m deep) supplied with flow-through seawater at 20 L min^{-1}, and fed 4 times daily on a mix of freeze-dried krill and commercial fish feed (2 mm sinking pellets, Skretting, UT, USA), at 0.4 g per individual per day. Fish constantly circled this tank as one large school. This work was conducted under Stanford IACUC permit no. 28859 for working on fish.

Creation of attack scenarios and looming animations

Three different models (Movie S3, Code S1) were played back to anchovies: 1) a constant speed simulation typically used in looming threshold experiments (6-10), 2) a model based on the mean anchovy-feeding (AF) data from (2) and 3) a model based on the mean krill-feeding (KF) data from (2). The constant speed scenario was a 2.8 s looming stimulus animation modelled on a disc the size of an average humpback whale's girth (2.65 m diameter) approaching at a constant speed of 5 m s^{-1} (Movie S3). AF and KF models were formulated using observed speed and engulfment parameters (timing of mouth opening and maximum gape) as well as size inputs from an average sized whale of 10.5 m length, with lower jaw max extension to 50°, upper jaw max extension to 30°, and with other characteristics including jaw length (2.25 m), whale diameter (2.51 m) and max girth location (4.41 m from the rostrum) allometrically or proportionally determined from the input length (11). Code S1 was used to create the looming animations using these parameters at a refresh rate of 60 Hz, such that the hypothesised viewing conditions from the prey perspective would be accurately recreated during playback. The stimulus is assumed to be perceived by the anchovies as a smooth animation of an approaching object, since the 60 Hz refresh rate is likely above that of the flicker fusion frequency of visual system of the prey. Although values of flicker fusion frequency of anchovies are not available, that of most fish species are below 60 Hz (12, 13).

For each frame of the model, the visual angle (α, Fig. 1) of the whale from the target's viewpoint was calculated as well as the rate of change of α (dα/dt). Up to a certain point in the model the apparent α of the whale is determined by its maximum girth and its distance from the target. However, the jaws of a humpback whale can extend beyond the whale's girth (in the 10.5 m whale length example the jaws can be up to 2.86 m wide). Thus, at the point when the combined viewing angle of the opening upper and lower jaws exceeds that of the maximum girth, α is determined by the combined angle and distance of the upper and lower jaws. For simulations of catch percentage (see below), if the whale approaches close to a fish school before opening its jaws, there can also be an intermediate point at which α is determined by a part of the whale anterior to the maximum girth. This scenario arises because although humpback whales are fusiform in shape they are not perfectly conical. In both the AF & KF playback experiments, however, the stimulus was constructed such that a fish located 16 cm from the screen would be reached by the virtual whale at the point when its jaws would be at maximum gape, and this point is far enough from the whale that α is not substantially different from the α of maximum girth until after the jaws dominate α (Fig. 1, S7a). Thus, for simplification in interpreting the playback experiment results, this intermediate α was excluded from the stimulus during playbacks but included in later simulations of catch percentage that involved schools of responding fish.

Escape Response Experiments

Escape response experiments were conducted in a 144 L glass tank (0.3 m wide, 1.2 m long, 0.4 m water depth), illuminated with LED strip lighting around its top edge. Three sides were covered with white board, with one long side left uncovered to allow side-view filming (Fig. 1). The entire tank and filming area were screened off from view using tarpaulins. A 17" LCD monitor was placed along the long side of the tank directly against the glass, visible through a cut-out in the screening. Two Edgertronic SC1 cameras (Sanstreak Corp, San Jose, California USA) were mounted in orthogonal positions, one directly above the midpoint of the width of the tank, the other at the side, positioned to capture part of the tank including the playback screen (Fig. 1). One camera was slaved to the other so that when triggered, 6 seconds of simultaneous footage preceding the trigger time was captured from both cameras at 250 Hz. Calibration videos were recorded before any experiments were conducted.

Fish were moved in groups of 7-9 individuals from the holding tank to the filming tank using a mesh net and observed for several minutes from a concealed position. Individuals which showed ongoing erratic behavior (e.g. swimming against the glass, darting) were removed to minimize disturbance to the remaining fish and placed in a separate holding tank. These individuals were not reused for any experiments. This left individuals which appeared to be in a calmer state (though with apparent heightened awareness) which typically swam up and down the length of the tank. These remaining fish were left for approximately 10 minutes further before being exposed to the looming animations. During this time, occasional videos were recorded of the fish turning spontaneously, and kinematic criteria to distinguish escape responses from spontaneous turns were independently established (see below). Occasionally fish manifested erratic behavior later in the trials, disturbing the other fish, and these individuals were removed as

above. As a result, responses were captured with different total numbers of fish in the tank, including some with only a single fish remaining.

Like other pelagic fish, anchovies are continuous swimmers and therefore looming animation video playback (which was between 3 and 4 s depending on the scenario) had to be timed so that in the course of their swimming patterns up and down the tank, a particular fish would view the animation in its entirety and also be close to the midpoint of the width of the tank, at the assumed viewing distance of 16 cm from the screen. Fish that were determined post-hoc to be more than 16 ± 3 cm from the screen at the time of response were excluded from analysis to maintain comparable apparent approach speeds. Fish were observed through a gap in the screening and the looming animations triggered manually when it was judged the swimming pattern of a particular fish might meet these criteria. Until playback was triggered, the screen displayed the initial frame of the animation, which in all scenarios consisted of a 3 cm black circle. This starting size was chosen so as to be relatively unobtrusive but also to make the animation a manageable duration so that playback could be timed correctly. When the animation was triggered, a live view from the camera was viewed on a laptop. If it was judged an escape response occurred, the video was saved. To maximise the chances of obtaining successful responses, and because correct timing of the animation to the fish position was extremely difficult, several playbacks of the animation were conducted for each group.

Escape response video processing

In total, approximately 350 anchovies were moved to the experimental tank for exposure to the looming animations. Over the three attack scenarios, a total of 130 anchovies demonstrated sharp lateral turns away from the screen coincident with animation playback. Of these recordings, 90 met the quality conditions for digitization. Of these, 30 (10 for the constant speed, 11 for AF and 9 for KF) met the criteria of being responses by unique individuals within ± 3 cm of the assumed viewing distance of 16 cm.

Overhead videos of potential escape responses were reviewed to determine the frame at which the response occurred, defined as the frame at which the specimen's turn away from the stimulus was initiated (Fig 1). The matching frame from the side-view video was used to identify the frame of the animation (and thus stage of the hypothetical attack) at which the response was initiated, via the frame indicator numbers visible on the playback screen (Movie S3). Overhead videos (Movie S5) were manually digitised using the DLTdv5 library for Matlab (14) to provide spatial XY coordinates. All further data processing was conducted in R. The XY coordinates were used to determine the turning rate of the fish away from the stimulus in $^\circ\ s^{-1}$. Turning rate was defined as the angular velocity of the anterior part of the body (represented by a line joining two digitised point, i.e. the tip of the head and a point at 20% of the fish's body length), between its position before and at the end of the turn (15). Twenty spontaneous turns were also digitized and turning rate of these likewise determined. The mean turning rate of the 30 escape responses used in analysis was $1166 \pm 389^\circ\ s^{-1}$, which clearly distinguished them from spontaneous turns (with turning rates $357 \pm 103^\circ\ s^{-1}$, n = 20). Spatial XY coordinate data, along with depth as determined from side-view videos, with data taken from calibration videos were used to determine the distance of the fish from the screen at the moment of the response.

For each escape response the frame of the looming animation at which the response was initiated was used to identify the associated $d\alpha/dt$ (the apparent LT) at which the

response occurred in the relevant attack scenario model. The calculated dα/dt in each attack scenario assumed a viewing distance of 16 cm when used to create the looming animation, but actual fish distances to the screen varied slightly from this, which affects the actual dα/dt experienced. To minimise this variability only responses which occurred 3 cm to either side of the hypothesised 16 cm viewing distance were used, and the dα/dt of each of these responses was adjusted for the viewing distance using the relationship:

$$\alpha = 2 \times \operatorname{atan} \frac{0.5 \times stimulus\ diameter\ on\ screen}{screen\ distance}$$

resulting in a mean apparent LT_{exp} of 2.05 ± 0.49 rad s^{-1}. Accounting for visual response latency (see below) resulted in a mean true LT_{exp} of 1.66 ± 0.37 rad s^{-1} (Table S1). The same calculations of α and dα/dt were applied to the response prediction models that utilized both metrics (Fig. S4).

Determination of visual response latency in anchovies

There is a lag between the brain sensing a stimulus and the body initiating a movement (6, 7, 10, 16). Looming animations continuously increase and as such do not typically provide an instantaneous moment of disturbance from which to measure neural lag, so to determine the actual dα/dt value of a response some assumed latency value must be applied. To estimate the latency between a visual stimulus and a physical response in *E. mordax*, experiments in which they were exposed to a sudden camera flash were conducted. Twelve trials were conducted in which individual anchovies were moved to a 1.5 m diameter tank. After 30 minutes, they were exposed four to five times to a camera flash, separated by 5 to 10 minute intervals, and filmed at 120 FPS using a GoPro Hero 4. Videos were reviewed for potential responses to the flash, characterized by either a sharp lateral turn, or rapid dash away in the direction of swimming. The frame at which the flash occurred was identified, and the video progressed frame by frame to identify how many frames after the flash that the initiation of the response was apparent. This was converted to a minimum latency duration in milliseconds. Of the 12 fish, nine showed a response to at least one flash. Those that responded to more than one flash (3 of the 9) were relatively consistent in their response times, varying by 2 frames (17 ms), 1 frame (8 ms), and 0 frames. For these three fish a mean latency between the two responses was calculated, for all others the single response latency was used, giving one latency value for each fish. The resulting distribution ranged from 33 to 88 ms and was non-normal (Shapiro-Wilk normality test, $n = 9$, $p = 0.005$), thus we applied the median latency value (61 ms) to calculated LT values.

Responses to the looming animations

All specimens in the AF and KF trials responded shortly after dα/dt increased abruptly, the moment of apparent mouth opening (AMO) simulating where the viewing angle (α) of the rapidly opening mouth surpasses that of the maximum girth (Fig. S5). Assuming a minimum response latency of 33 ms, the lower end of the range estimated in the response latency estimation experiments, all responses occur after this moment (Fig S2, column 2). Any single latency value higher than this applied to all specimens, e.g. the mean or upper end of the range established in the response latency estimation experiments (61

and 81 ms respectively), would mean some specimens appear to respond before the mouth opens. However, since we did not see any responses in the constant speed (CS) trials at $d\alpha/dt$ values this low (< 0.23 rad s^{-1}), the parsimonious explanation is that these specimens are instead responding at latencies on the low end of the calculated values (~33 ms). Overall, the placement of responses in these two scenarios are consistent in suggesting that fish are responding to a similar LT range as established in the CS scenario. Moreover, they illustrate how the characteristics of whale attacks compress the range of LT_{exp} into a very brief moment at apparent mouth opening, such that any escape response by the targets to values in the LT_{exp} range will occur within a brief, predictable temporal window during the attack.

This finding of a narrow temporal window encompassing the calculated response thresholds but a relatively wide range of response times after the stimulus threshold is passed differs from previous work largely due to the nature of the approach stimulus. That is, previous work that used looming approaches to trigger escape employed stimuli that changed size smoothly whereas our approaches were constructed from measured predator data and had a defining point of inflection with a rapid increase in stimulus size coincident with mouth opening. This rapid increase is similar in effect to an approaching predator that exhibits sudden accelerations. Our results suggest that fish may have delayed responses to such events, which may in turn explain why many predators, such as sea lions and whales, do not approach schools using smoothly increasing speeds but instead vary their speed and attack angles within an approach.

The variation in response timings after AMO, which was as high as 300 ms (Fig. S5), is not fully explained by individual variation in visual response latency which we observed to range from 33 to 88 ms. To investigate further properties of the stimulus that may influence response reactions, we additionally investigated if response models based only on stimulus size (α) regardless of attacker speed would explain the results (17). However, the α values for AF/KF at response were significantly lower ($p = 0.002$) than in the CS trials, which made it clear that this was not a credible response model. Next we investigated if response models based on the rate of increasing stimulus size ($d\alpha/dt$), but that incorporated an inhibitory function of α (18, 19) would better explain the observed responses than models based only on $d\alpha/dt$. All of the models tested had similar variability in response timing (200-400 ms) (Fig. S4), so none of the models better explained the observed variation (Fig. S4). Therefore, when the response models were applied to attack simulations to calculate catch percentages (see below), both a "quick response" scenario using the median visual response latency (61 ms) and a "slow response" scenario with an additional 200 ms delay were used to bound the predictions of how many anchovies could be captured by a lunge feeding event.

Anchovy escape speeds

To determine the speeds at which anchovies flee, laboratory trials were conducted in which small groups were filmed in a large tank escaping from a mechanical stimulus (the far end of a broom handle touching the surface of the water), and the acceleration and speed of individuals (n = 12) was determined over 1 s to 1.33 s (Fig. S6). Typical escape swimming behavior was a rapid acceleration from almost stationary to between 2 and 3 m s^{-1} in approximately 0.3 s (consistent with other fish within this size range (15, 20)), followed by maintenance of this speed or slight deceleration. Maintenance of initial burst

speeds for ~ 1 s is common in non-pelagic species (21) before deceleration to ~ 1/2 speed. In our case, because the natural deceleration could not be separated from deceleration because of the tank walls, the final speed was assumed to be maintained through the duration of a humpback's gape cycle. The fastest mean fish, and the mean of all fish were used separately as inputs into the model.

Simulations of capture efficiency

The min (0.89 rad s^{-1}), mean (1.66) and max (2.06) LT_{exp} of response, and the min, mean and max anchovy escape speeds (Fig. S6) for five different escape trajectories that encompassed the range of theoretical responses (see below) were used to construct the probabilities that fish in a school would escape from an approaching 10.5 m humpback whale with max girth 2.5 m located 4.41 m behind the front of the whale with 2.25 m jaws (the same whale size assumed in the looming threshold experiments). For results reported in Figs. 3 & 4 we assumed that anchovies fled the predator at the mean escape speed observed in the lab (accelerating from 0 to 2.3 m s^{-1} in 0.3 s and maintaining that speed through the escape, Fig. S6). While a humpback whale's shape can be approximated by a cone with the maximum girth visible to the prey for most of the approach (Fig. 1A), at close viewing distances (< 1 m) the maximum perceived projection of the whale may instead be a part of the animal more anterior than the maximum girth. These real-life shapes were accounted for in simulations of fish responses to predator approaches, and the non-ideal shape of humpback whale, blue whale and sea lion predators were estimated from profile and overhead images of each species. These shape parameters are reported in the supplemental R and Matlab codes.

The tested approaches followed the mean Type 1 and Type 2 speed and engulfment profiles shown in Fig. 4, with mean engulfment calculated as distance from the first inflection point of the speed profile after the max speed. We constructed models assuming both that fish responded directly to the stimulus of the approaching whale or would respond instead to the reactions of the fish around them (22). In the second case, the response was modeled as if the school responded in a wave moving away from the initial stimulus at 6.7 m s^{-1} (23). Any fish located more than 24 cm (two body lengths) away from the edge of the school was assumed to respond to the school as the line of sight to the approaching predator was likely obstructed. To encapsulate the observed variation in humpback whale approaches, in the model tests we alternately varied the distance from the school at which the whale would open its mouth, the timing of the mouth opening event along the speed profile, and also multiplied the speed of the SoCal approach by factors from 0.1 to 3. In all cases, the timing of maximum engulfment and overall engulfment duration were scaled using calculations from (2) such that the overall volume of water engulfed would be consistent.

For any given humpback whale engulfment profile α and $d\alpha/dt$ were calculated from the viewpoint of theoretical target fish at every time step (at 60 Hz) along the whale's approach using the LT model (Code S1). Then, for a given LT at which the fish respond, the time from the whale reaching this LT for each fish in a school to when the whale's jaws would reach the fish was calculated for each of 5 different potential prey escape trajectories:

1) A perpendicular escape trajectory in which all fish flee in a direction directly perpendicular to the oncoming whale's trajectory
2) Like #1, but assuming that all fish fleeing laterally are flushed back towards the mouth by the flippers (24, Movie S4) and consumed. We calculated the percentage of fish that would additionally be caught if fish fleeing to the outside of the school perpendicular to the whale's path were instead corralled by the flippers back towards the mouth and engulfed (Figs. 2d, 4). In this scenario, at least 50% of fish would be caught every time. This appeared to be the least realistic scenario.
3) An angled escape calculated from the instantaneous ratios of the whale's speed and the anchovy escape speed as $180° - \text{acos}(U_{prey}/U_{pred})$ (25), where 180° is directly away from the predator. These values varied from 101° to 180° (either to the left or right) and are the most likely initial escape trajectories based on published work on clupeoid fish (25-27).
4) Like #3 but with the horizontally fleeing fish flushed back towards the mouth
5) An escape directly away from the oncoming whale along the same trajectory. In this scenario if the whale is faster than the fish, all fish are engulfed, and if the whale is slower all fish escape.

The "escape distance" each fish would be able to travel perpendicular to the whale's approach in the time before it was reached by the whale's jaws was calculated. For every fish in a disc perpendicular to the whale's attack, their "safe distance" was the distance that fish had to travel horizontally (perpendicular to whale approach) to be outside a space the area of the whale's jaws. If a fish's escape distance did not exceed the safe distance, the fish was assumed to be engulfed. The percentage of fish at each time step that could escape was then summed and standardized for the size of the whale's mouth at each time step, and a total catch percentage was calculated. As escape scenarios 3 & 4 are the most likely scenarios, they are reported in Figs. 2-4. Other escape scenarios had increased catch percentages but similar trends in the importance of timing. Similarly, only the scenario using mean LT_{exp} is reported in the figures, but no substantial differences were found when using min or max LT_{exp} as all were nearly coincident in all models where the whale opened its mouth.

For all catch percentage simulations run, the size of the fish school was assumed to be larger than the engulfment volume of the whale such that if the fish did not flee, the whale's mouth would be full of fish at their schooling density. At each time step, fish in the school were assumed to be evenly distributed in a plane perpendicular to the oncoming whale in two semi-circles – one with radius of the vertical projection of the upper jaw at that time ($Length_{jaw} \times \sin(JawAngle)$) and one with radius of the vertical projection of the lower jaw.

For results presented in Figs S1 and S2, the escape responses of fish to the LT_{exp} was compared to the escape responses given a model that assumes an inhibitory effect of loom size (α) using the equation $\eta = \alpha \times e^{-2.576\,\alpha'}$, where $\alpha' = d\alpha/dt$ (see Fig S4 for details on model construction). Figs S1 and S2 also model catch percentages assuming that fish respond in the wild nearer to the slower responses we observed to AMO. Catch percentages thus range between the maximums for the quicker and the slower observed responses.

Additional predator capture efficiency

To compare how anchovy escape responses to attacking humpback whales compares to both larger whales and to particulate feeding predators, varying size inputs and speed/engulfment profiles were input into the dα/dt profile code (Code S1). For the blue whale simulation, we used the mean speed profile from (2) and a mid-sized 22.8 m long blue whale with 3.1 m girth diameter and max girth placed 20% behind the rostrum. For a predator foraging on single prey, we simulated the California sea lions (*Zalophus californianus*) observed to feed in concert with the whales in this study (Movies S1, S2, S4). We measured a medium sized sea lion from overhead imagery as 1.67 m with 0.55 m girth diameter located 32% of body length behind the snout. An average sea lion has jaws 6.3 ± 1.4 cm wide (28) which can be used to interpret the likelihood of a fish's escape. Although the approach speed of sea lions is not precisely known, we chose constant approach speeds (3.5 and 5.5 m s^{-1}) that span the range of typical to extreme sea lion speeds (29, 30), as well as the approach profile of a blue whale to examine how the influence of size alone affects anchovy perceptions of predators.

Given these inputs, we calculated when an approaching predator would exceed the mean LT_{exp} for a fish that is initially located at the spot at which a whale would reach maximum gape or at which a sea lion would reach maximum speed. For the whales, catch percentage was determined as above. For the sea lion, horizontal escape distance of the fish was calculated by determining the ideal escape angle for the fish to flee as in scenario (3) above, a latency of 61 ms was applied, and then the mean escape speed as well as the mean ± 1 SD escape speeds were applied. Results are displayed in Fig. S7. In all sea lion cases, the LT of anchovy response occurred before the sea lion would arrive at the fish. In all whale cases, the LT of response occurred after the whale would have already opened its mouth.

Humpback whale foraging efficiency

The surplus efficiency of a lunge (Fig. 4) was calculated as $(E_{in} - E_{out})/E_{out}$. Estimates of metabolic expenditures (E_{out}) are based on calculating the energy spent by the locomotor and ventral groove blubber (VGB) musculature during the energetically most significant stages of a feeding lunge, namely pre-approach and engulfment as detailed in (31). These calculations are based on the use of tag data as input in a calculation of the mechanical energy, which is then corrected by propulsive and metabolic efficiency constants to yield the sought-after metabolic expenditures (32-36). The mechanical expenditures by muscle are obtained from the work-energy theorem applied to the whale's body in which changes in kinetic energy are expressed in terms of the energy loss through drag generation and/or gained via fluking. This approach has been used previously for estimating the energetics of the engulfment stage during lunge-feeding for krill by blue whales (37), and has been generalized to include fluking-induced accelerations in both prey-approach and engulfment stages (as detailed in 31). Energy during acceleration was thus determined as $\frac{\Delta KE}{\gamma_1\gamma_2} + robMR \times (t_2 - t_1)$, any coasting or deceleration from drag was $robMR \times (t_2 - t_1)$, and any work done during engulfment by the VGB was $\frac{M_c}{2\gamma_1\gamma_3}(v_{higher}^2 - v_{lower}^2)$, where ΔKE takes into account any changes of mass from engulfment, γ_1= metabolic efficiency (0.25), γ_2 = propeller efficiency (0.8), γ_3 = extra muscle use efficiency (0.9), *robMR* = Rest of body metabolic rate = $1.6 \times 4.1\, M_c^{0.75}$ (31,

38, 39), t_2 and t_1 are the times (in s) at the end and the beginning, respectively, of the period of interest, M_c is the mass of the cetacean (pre-engulfment) and v_{higher} and v_{lower} are the start and end velocities, respectively, during deceleration or the end and start velocities during acceleration. M_c was calculated using the ordinary least-squared scaling equation for a 10.5 m whale (11). Matlab code to calculate energy expenditure from speed and engulfment data is available as Code S2, and as a first approximation, the overall energy used by foraging humpback whales can be estimated using a quadratic model ($r^2 = 1.000$): $E = 0.01966x^2 + 0.1066x + 0.3895$ where E is energy in MJ and x is maximum speed of the lunge (Fig. 3a).

For all scenarios, the energy from successfully engulfed prey (E_{in}) was calculated as $E_{in} = V_{engulf} \times fish\ density \times energy\ density$, where V_{engulf}= engulfed water mass (11) divided by the density of sea water (1027 kg m^{-3}), and a representative *fish density* of 7.8 kg of fish per cubic meter of water (based on length-weight relationships from (40), a school packing density of 1 body length cubed per fish (41, 42), and a representative fish length of 12 cm) and *energy density* of 6 MJ/kg (43, 44). This value was then scaled by the percentage of fish caught (Fig. 3).

For the Type 1 whales that utilized high speed approaches to dolphin-associated schools that were typically smaller than a whale's engulfment volume, the mean school size was generally smaller than a whale, averaging ~ 1 m in diameter (the length of a common dolphin, Movie S2). A scaling factor of 29% could thus be applied to E_{in} (and then applied to the storage efficiency equation) for applications in energy acquisition modeling. Because the point of these exercises was to compare the engulfment energetics of different engulfment scenarios, this scaling factor was not applied in Figs 3 and 4.

Humpback whale AF and KF feeding rates

To compare foraging rates of AF and KF whales, we identified all lunge-feeding events from the tag records of the AF whales in this study as well as seven additional KF humpback whales from Monterey Bay, CA tagged 2016-2018 using CATS tags. Lunge rates from these seven were combined with lunge rates from 4 other published records in California (2, 45). Only California whales were used for comparison to AF whales so as to include only sympatric whales that could theoretically choose to feed on anchovies or on krill. Lunge-feeding events were identified from the tag records as peaks in speed with rapid deceleration (2) that correspond to increases in |jerk| (46) as well as changes in pitch, roll and heading associated with maneuvering. Reported results are feeding rates for the duration of the AF deployments all of which only spanned daylight hours (mean deployment time: 3.3 ± 2.6 hrs, max: 7.9 hrs). KF deployments were broken into daylight or night time to account for diurnal variation in feeding behavior and reported results are the means of either daylight feeding rates for (10 of 11 deployments that were daylight feeding dominant) and the night time feeding rate of the whale that was night time feeding dominant. For comparisons of E_{in} between AF and KF lunges, anchovy parameters were as in the storage efficiency calculations, and krill patches were assumed to be consumed with low escapement (90% catch), to have an energy density of 3.8 MJ kg^{-1} (47) and to be engulfed at an approximate average density (1 kg m^{-3}) observed from echosounder data in California collected concurrently with tagged KF whales.

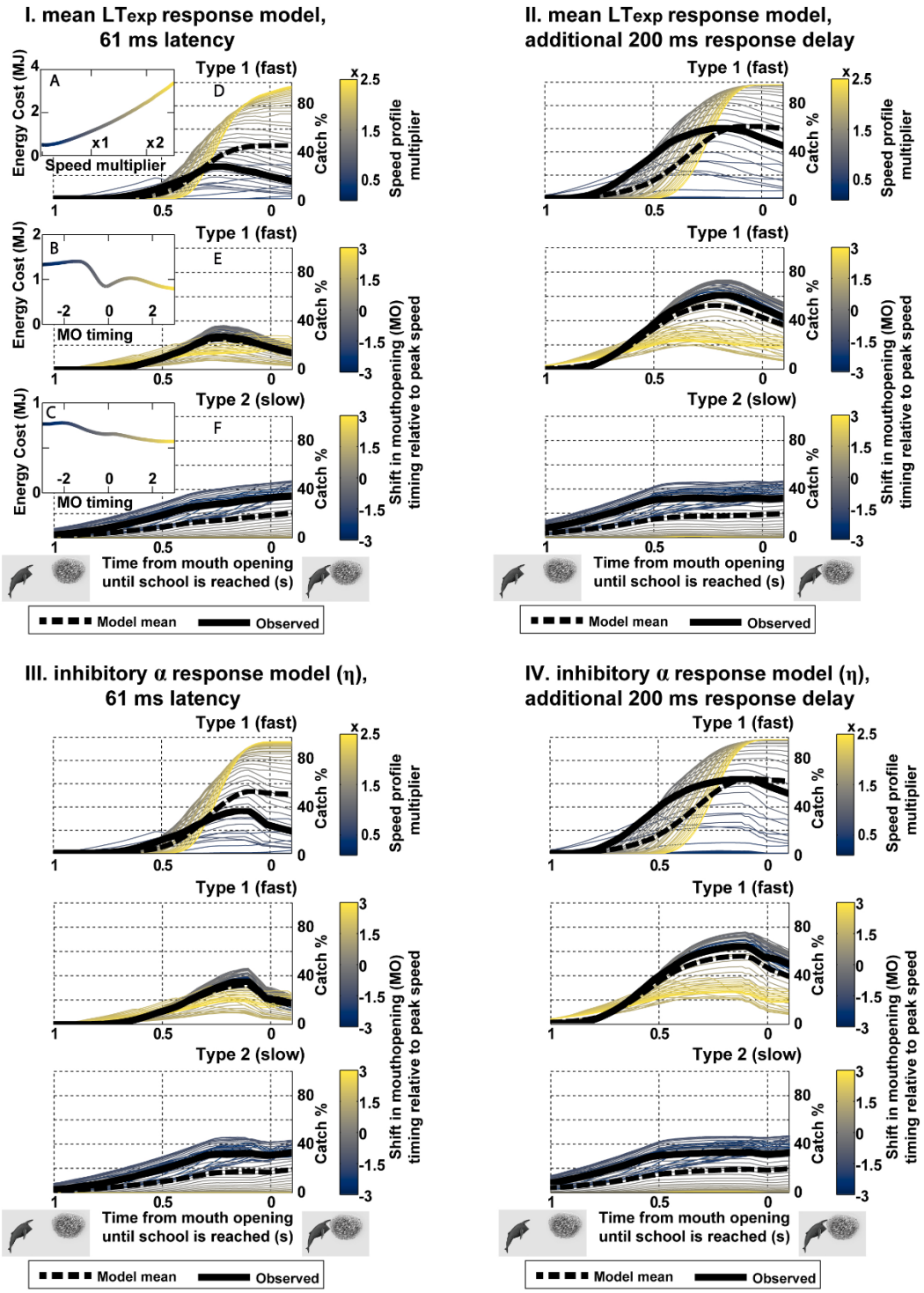

Fig. S1- Modeled catch percentages based on different response scenarios. See Fig. 3 caption for more details. I) same as Fig. 3. This is the dα/dt threshold with 61 ms latency applied. II) The dα/dt threshold model with 261 ms latency applied. This is the maximum expected catch if fish respond in the wild at the slower responses observed in the lab. III) Modeled catch percentage assuming the response to looming rates are inhibited at large α (η model described in Fig. S4). IV) Modeled catch percentage for the η model and using a 261 ms latency.

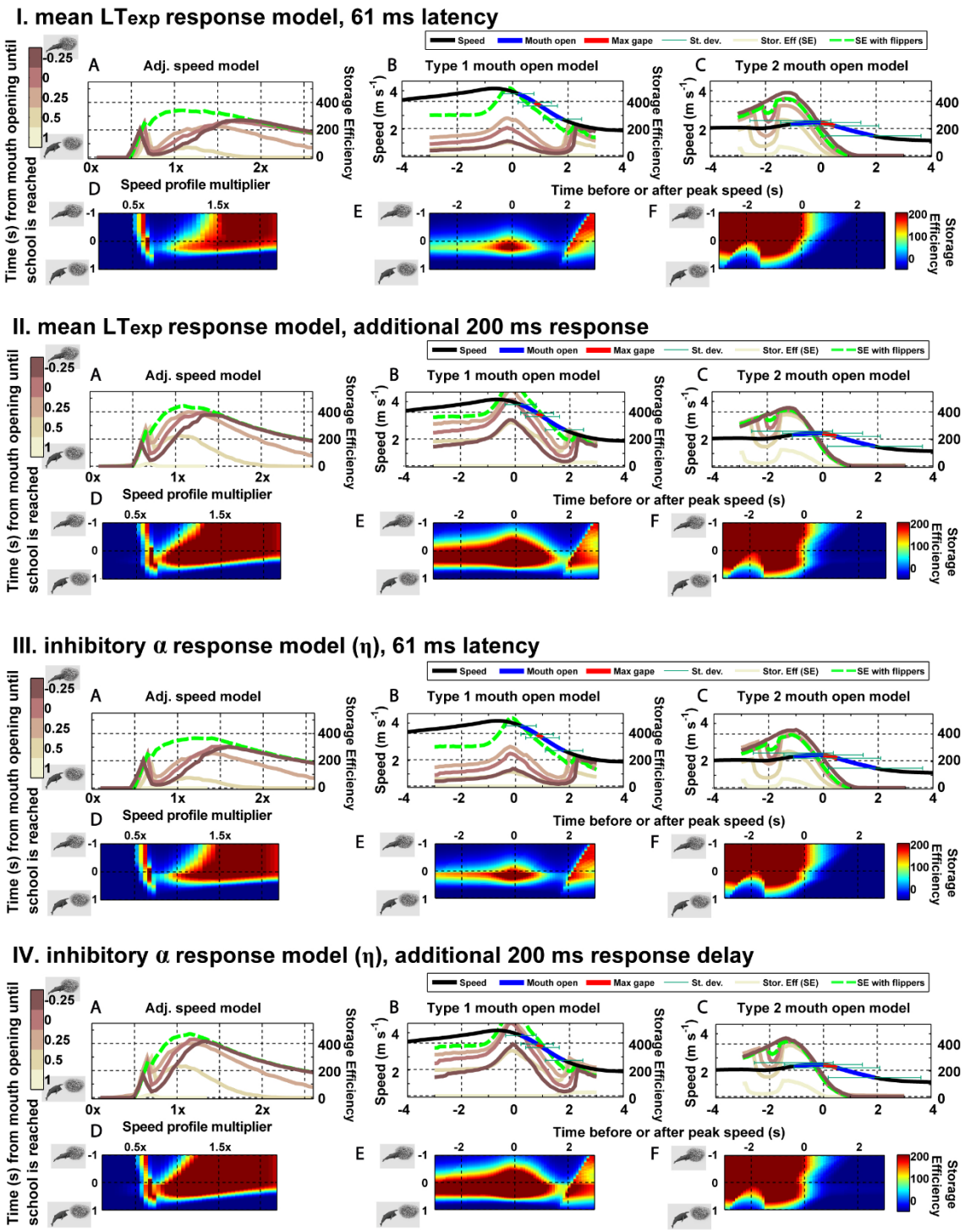

Fig. S2- Modeled foraging efficiencies (surplus efficiency) based on different response scenarios. See Fig. 4 caption for more details. I) same as Fig. 4. This is the dα/dt threshold with 61 ms latency applied. II) The dα/dt threshold model with 261 ms latency applied. This is the maximum expected catch if fish respond in the wild at the slower responses observed in the lab. III) Modeled catch percentage assuming the response to looming rates are inhibited at large α (η model described in Fig. S4). IV) Modeled catch percentage for the η model and using a 261 ms latency.

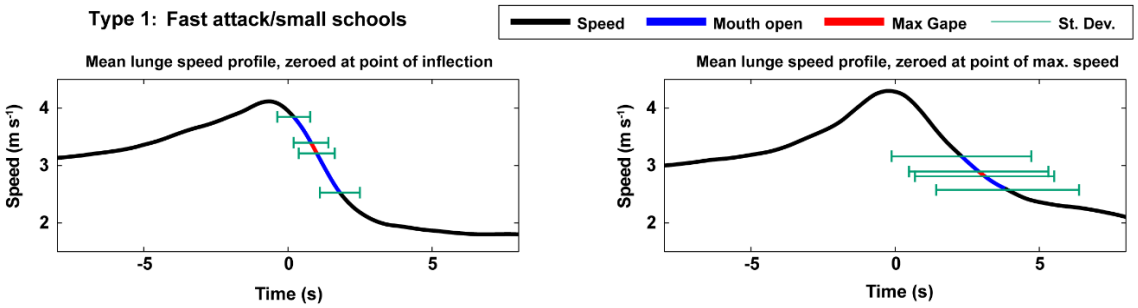

Fig. S3- The engulfment timing and speeds of tagged anchovy-feeding whales in SoCal were faster and more consistent in timing than previously reported fish-feeding humpback whales, and were similar in character, with engulfment consistently coincident with the rapid deceleration phase, to previously reported krill-feeding rorquals (2). A) the mean speed profile (also displayed in Fig. 1 and Fig. 4B) of 84 lunges from 9 whales, centered around the timing of rapid deceleration onset where mouth opening is 0.2 ± 0.6 s after this point of inflection. In many cases, this point was not coincident with peak speed as many whales started decelerating before mouth opening. B) When the same data are centered around peak speed, engulfment timing is much more variable, implying that the point of inflection is a result of deceleration from the high drag of engulfing a water mass that can exceed body mass (11).

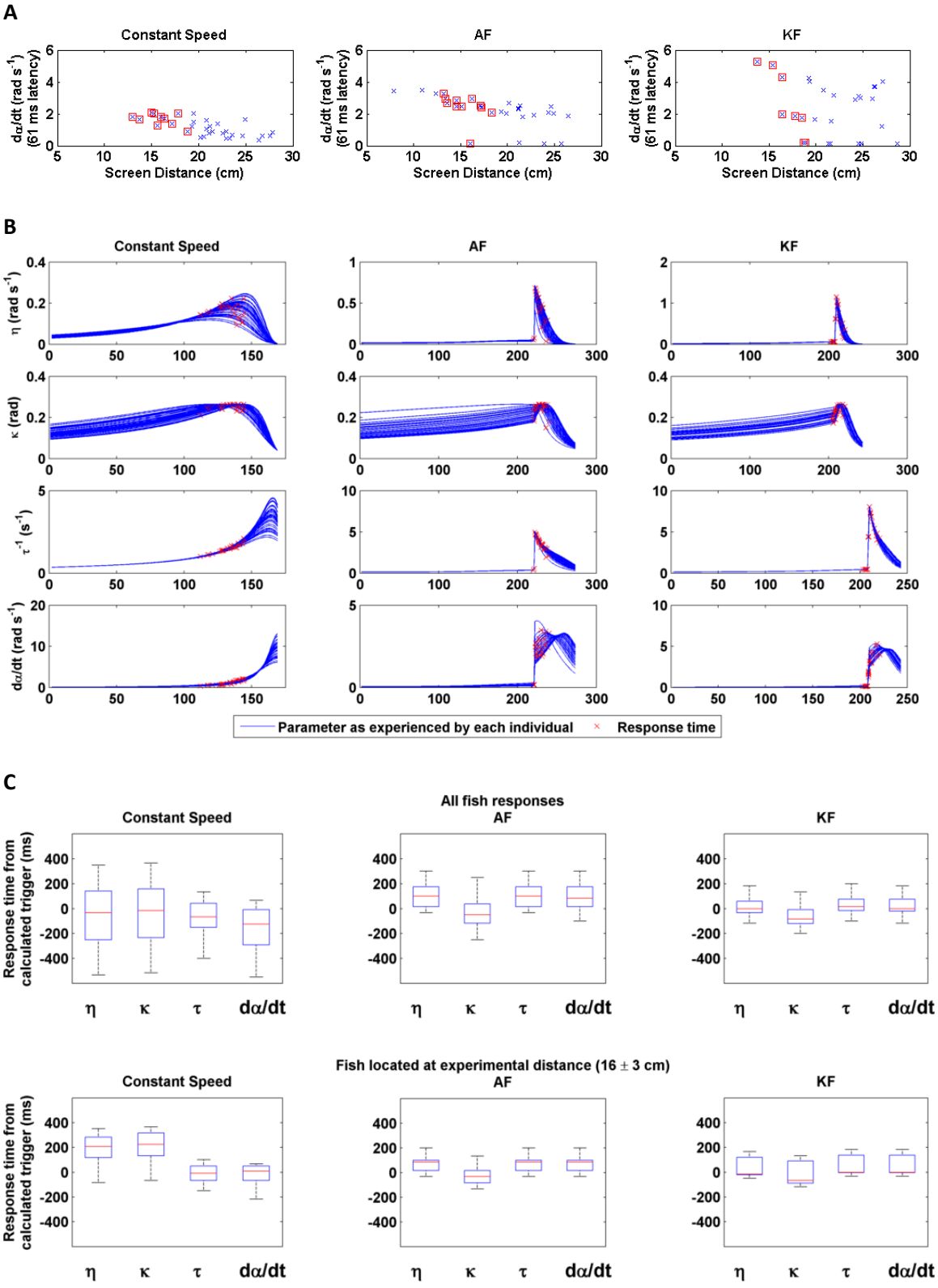

Fig. S4- Summary of stimulus response interpretation models, as formulated in (19). In all panels, $\alpha' = d\alpha/dt$, $\eta = \alpha \times e^{-2.576\,\alpha'}$, $\kappa = \alpha \times e^{-1.393\,\alpha}$, $\tau^{-1} = \alpha'/\alpha$ and all panels applied a

neurological latency of 61 ms. The constants in the formulations of η and κ were derived by finding the global value that minimizes the squared difference in the time of the observed responses during the constant speed experiment from the maximum of the curves. A) LT of response for every fish in all three playbacks as a function of distance from the screen. The decreasing slope of responses suggests that response to dα/dt may be inhibited by larger α. Only data points with red boxes (fish within 3 cm of the intended 16 cm distance) were used in further analyses. B) Responses of each fish plotted on its observed line (lines differ based on different screen distances). C) Variation in anchovy response timing for all three stimulus experiments using all four stimulus interpretation models. While there is slightly less variation in the τ and dα/dt threshold based models in the constant speed experiments, no model does a better job of explaining the variation in response timings in the real approach speeds, suggesting there are additional factors besides loom rate (dα/dt) and loom size (α) that influence response timing.

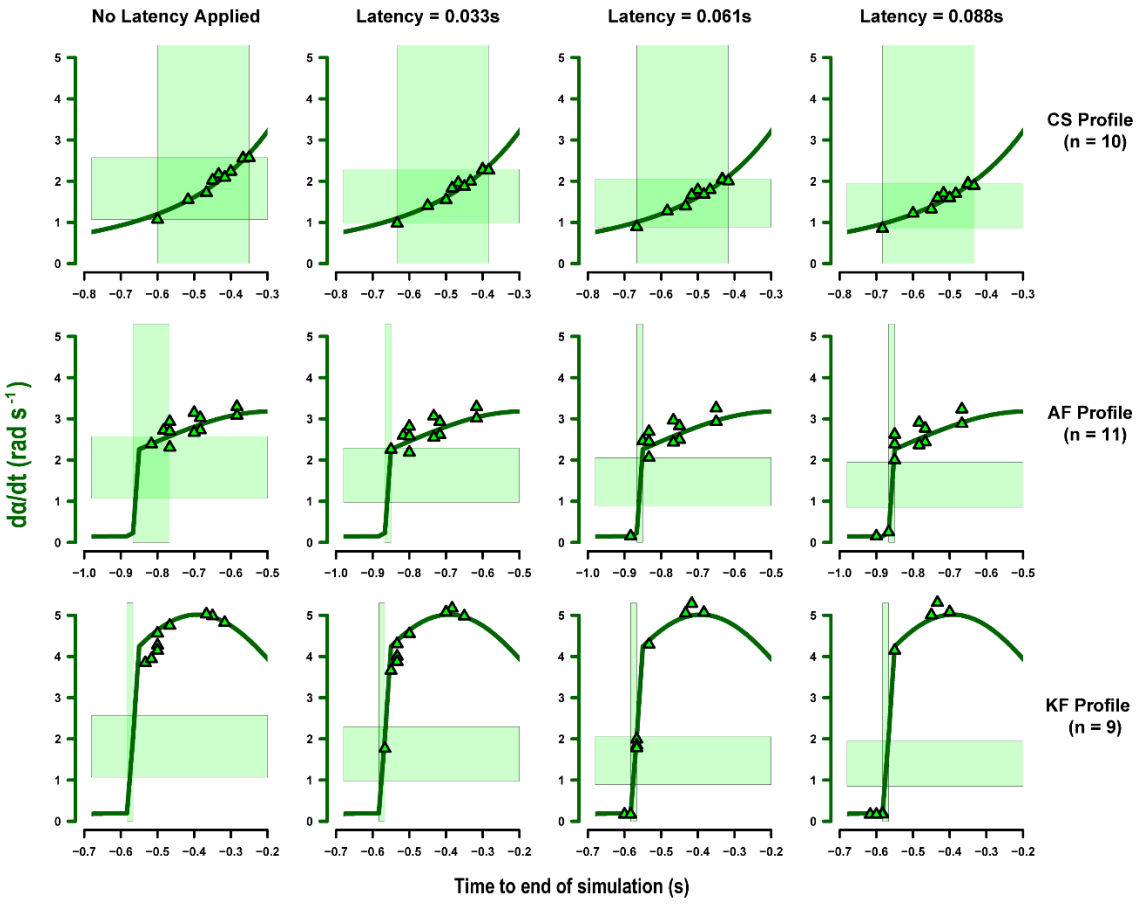

Fig. S5- Anchovy escape response timings (triangles) in each of the three looming animation trials (CS = constant speed, AF = anchovy feeding, KF = krill feeding) in relation to dα/dt with the experimental range of neural response latency values applied. Horizontal axes represent a 0.5 s window containing all responses. The green line represents changes in looming stimulus dα/dt as observed from the assumed viewing distance of 16 cm (only fish that were within 3 cm of this distance at the time of response were included in our analyses). Vertical offset of points from this line result from corrections to each fish's observed dα/dt due to deviations from the assumed viewing distance. Green shaded regions indicate the lower to upper range of LT_{exp}, based on applying that column's latency to the CS profile, as well as the time period over which this occurred. In the CS trials this range occurs over approximately 0.25 s while in the trials modelled from whale kinematic and engulfment data, it is compressed into a single animation frame once latency is applied. The potential for delayed responses to stimulus crossing is apparent in the AF and KF trials as some fish responded 200-300 ms after AMO. The delayed response models in Figs. S1 and S2 account for the potential for these longer response times to be conserved in the wild.

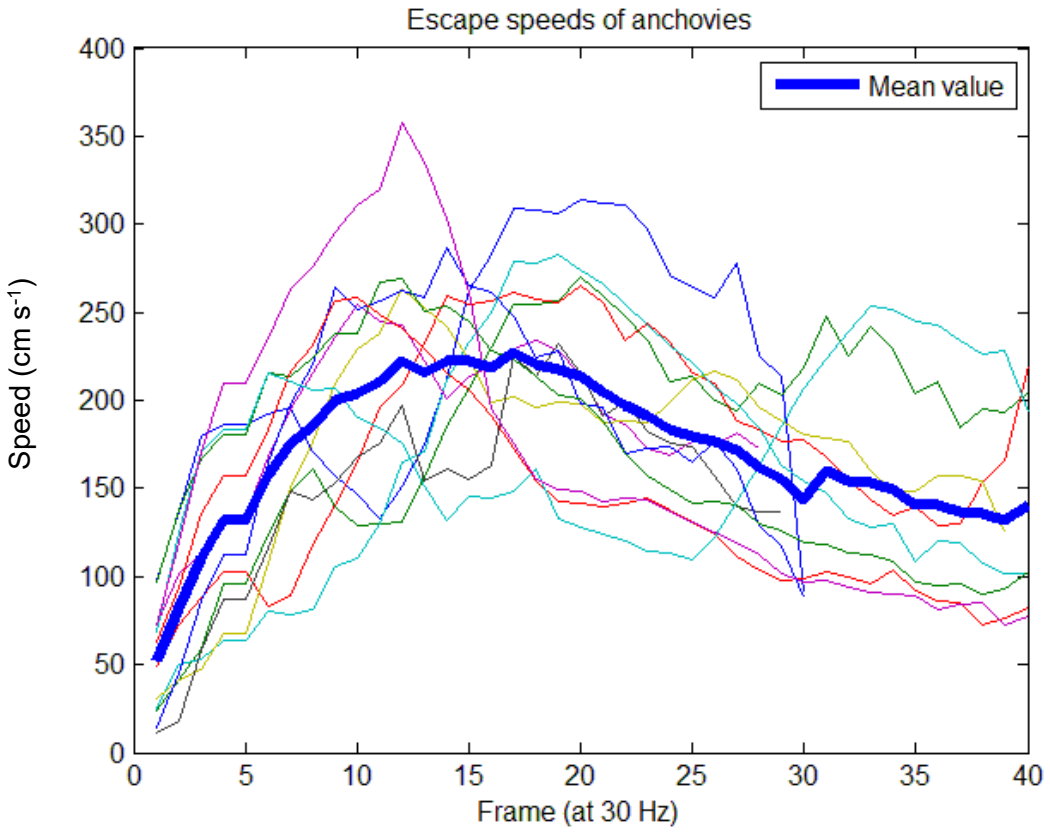

Fig. S6- Speeds of 12 anchovies fleeing a mechanical stimulus recorded with a high speed camera.

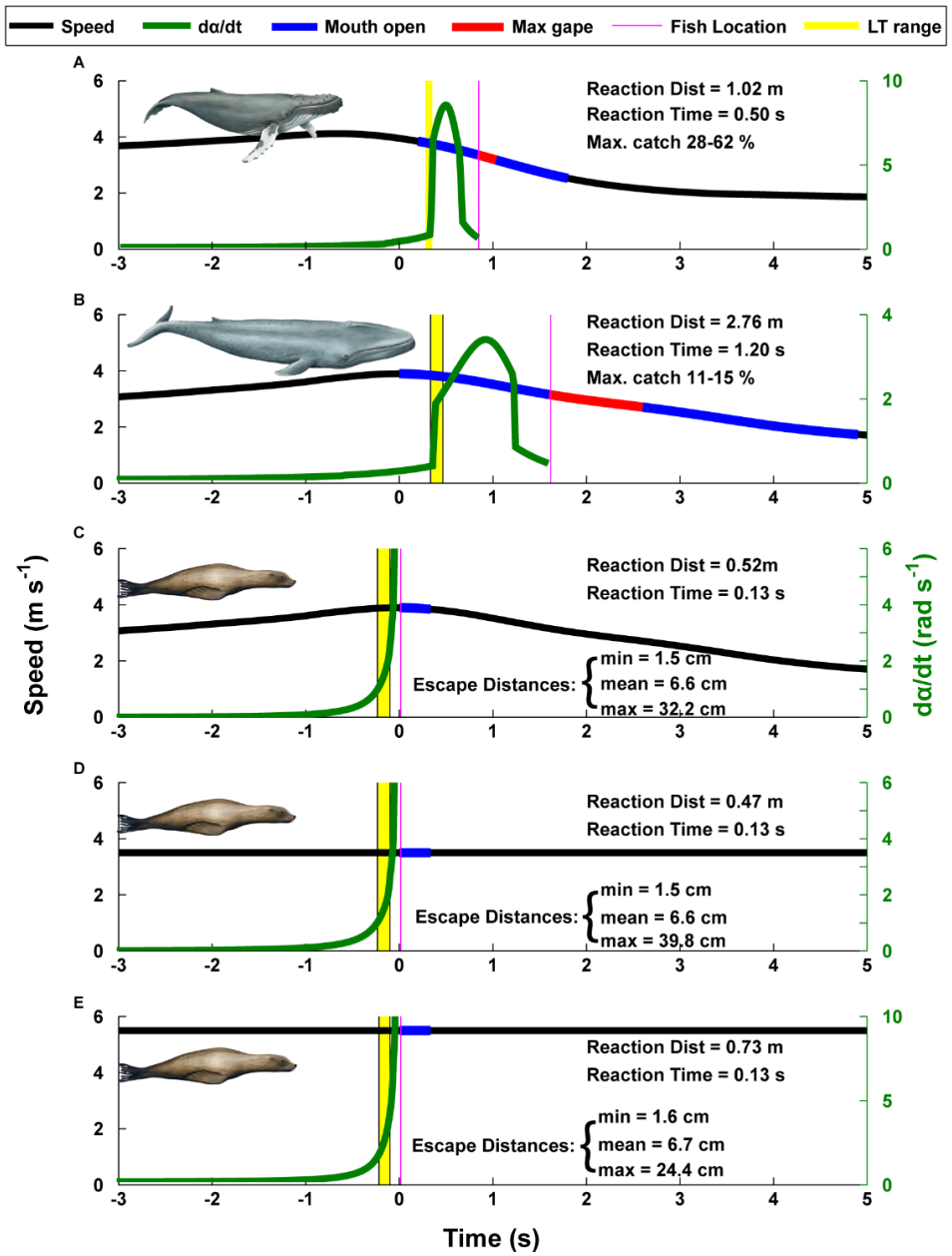

Fig. S7- Approach simulations based on speed (black) and mouth opening (blue/red) that result in looming stimuli changing size at dα/dt (green). A) The Type 1 humpback approach profile- min/mean/max LT_{exp} are all reached simultaneously for a fish that would be reached at maximum gape, but after the whale has already opened its mouth. Max catch range is based on slow and fast response times (Fig. S5). B) A simulated blue whale approach, the long engulfment time means more fish have a chance to escape. C) A sea lion approach using a blue whale speed profile but with a sea lion's size. D) A constant speed (3.5 m s^{-1}) approach of a sea lion sized predator. E) A faster constant speed sea lion approach (5.5 m s^{-1}). In sea lion scenarios, all LT_{exp} are reached before the sea lion reaches the prey. Escape distances are how far an anchovy would be able to travel horizontally before being reached by the jaws of the sea lion. Min = late detection (max LT_{exp}) and slow escape (mean fish escape speed – 1 SD), mean = mean LT_{exp} and mean escape speed, max = early detection (min LT_{exp}) and fast escape (mean + 1 SD).

Table S1- Anchovy looming stimulus experimental results of fish that were within 3 cm of the assumed 16 cm screen distance (30 fish total). CS = constant speed, AF = anchovy feeding, KF = krill feeding. A looming stimulus that represents a predator typically gets bigger by getting closer to the prey, however a rorqual whale has an uncommon approach in that it also expands its profile when the jaws extend past the maximum girth at apparent mouth opening (AMO), implying that an anchovy may perceive this threat as approaching much more rapidly (final column) than the modeled speed. (1) Distance from screen at moment of response (cm), (2) Time from AMO until response (s), (3) Apparent LT of response ($d\alpha/dt$ in rad s^{-1} corrected for screen distance), (4) True LT of response ($d\alpha/dt$ in rad s^{-1} after applying median neurological latency), (5) Modelled speed (m s^{-1}) at moment of response (0 latency), (6) Perceived speed (m s^{-1}) at moment of response (0 latency). If results for fish not within 13-19 cm of the screen (<13 cm, n = 3, >19 cm, n = 57) are included in analysis, no substantial difference in timing of response was noted (fish still respond within ms of the AMO event).

Specimen	Scenario	(1) Distance from screen (cm)	(2) Time from AMO (s)	(3) Apparent LT (rad s^{-1})	(4) True LT (rad s^{-1})	(5) Modelled speed (m s^{-1})	(6) Perceived speed (m s^{-1})
CS01	CS	13.02	n/a	2.16	1.79	5.0	4.1
CS02	CS	13.75	n/a	2.02	1.66	5.0	4.3
CS03	CS	15.00	n/a	2.56	2.06	5.0	4.7
CS04	CS	15.22	n/a	2.55	2.04	5.0	4.8
CS05	CS	15.67	n/a	1.55	1.28	5.0	4.9
CS06	CS	16.03	n/a	2.24	1.79	5.0	5.0
CS07	CS	16.36	n/a	2.09	1.68	5.0	5.1
CS08	CS	17.20	n/a	1.72	1.39	5.0	5.4
CS09	CS	17.86	n/a	2.57	2.00	5.0	5.6
CS10	CS	18.80	n/a	1.07	0.89	5.0	5.9
AF01	AF	13.18	0.27	3.29	3.26	2.1	5.3
AF02	AF	13.34	0.15	3.15	2.97	2.2	9.3
AF03	AF	13.55	0.08	2.93	2.69	2.2	14.0
AF04	AF	14.54	0.07	2.72	2.46	2.2	16.8
AF05	AF	14.61	0.17	3.03	2.83	2.2	9.4
AF06	AF	15.08	0.08	2.70	2.45	2.2	15.6
AF07	AF	16.03	0.03	2.39	0.15	2.2	23.4
AF08	AF	16.26	0.27	3.08	2.93	2.1	6.6
AF09	AF	17.17	0.17	2.73	2.50	2.2	11.0
AF10	AF	17.22	0.15	2.67	2.43	2.2	12.0
AF11	AF	18.30	0.08	2.31	2.06	2.2	18.9
KF01	KF	13.71	0.22	4.98	5.28	2.6	6.0
KF02	KF	15.38	0.25	4.82	5.07	2.6	5.5
KF03	KF	15.42	0.20	5.03	5.05	2.6	7.5
KF04	KF	16.37	0.07	4.56	1.99	2.7	23.7
KF05	KF	16.43	0.10	4.75	4.29	2.6	17.0
KF06	KF	17.81	0.07	4.27	1.84	2.7	25.8
KF07	KF	18.51	0.07	4.14	1.78	2.7	26.8
KF08	KF	18.66	0.03	3.84	0.17	2.7	40.0
KF09	KF	18.90	0.05	3.94	0.17	2.7	33.0

Movie S1- Anchovy schools disperse when attached by humpback whales, while krill schools do not show an apparent escape response. Although this is a single example, coordinated escape by krill has not been observed in any of hundreds of lunges from whale-borne camera footage. High-quality version available at: https://purl.stanford.edu/mt574ws5287

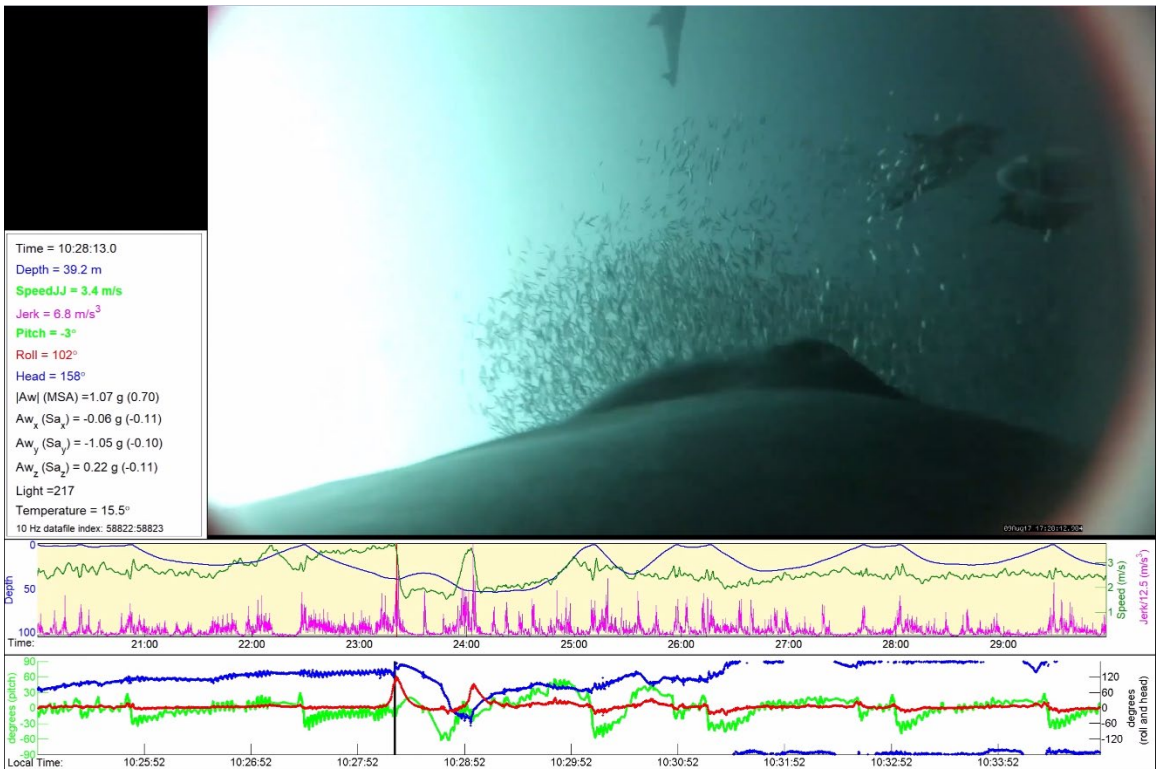

Movie S2- Humpback whales in the study from Southern California (SoCal) fed at high speeds on small schools in concert with common dolphins (*Delphinus sp.*). A humpback whale from Monterey Bay, California fed at slower speeds on a large school in concert with California sea lions (*Zalophus californianus*). High-quality version available at: https://purl.stanford.edu/mt574ws5287

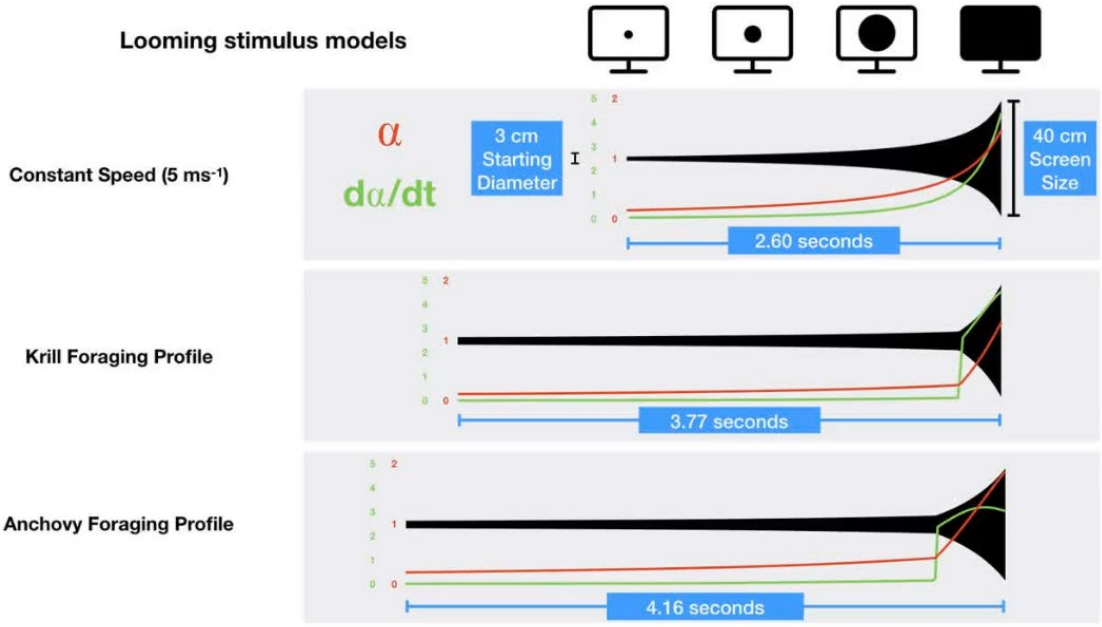

Movie S3- The visual stimuli used to test the escape responses of anchovies (*Engraulis mordax*). The stimuli parameterized from predator data had delayed and then rapid expansion of the stimulus. Times in the screenshot above refer to times from the start of the simulation until the screen is completely filled.

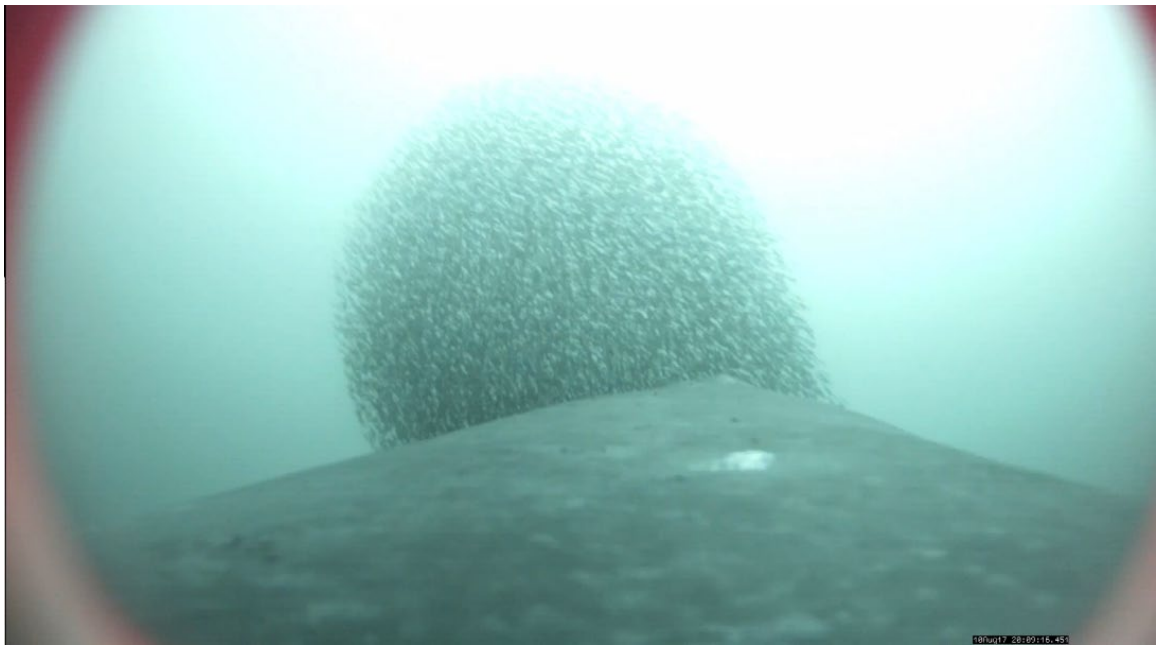

Movie S4- Humpback whale flippers are extraordinarily long (~ 30% of body length (11)) with white bottoms, and attacking whales regularly rotate and extend them when lunge-feeding, a technique that has been shown to have a startle effect on prey (24). When humpback whales approach prey but do not open their mouths, schools maintain formation since the threshold of response is not reached. High-quality version available at: https://purl.stanford.edu/mt574ws5287

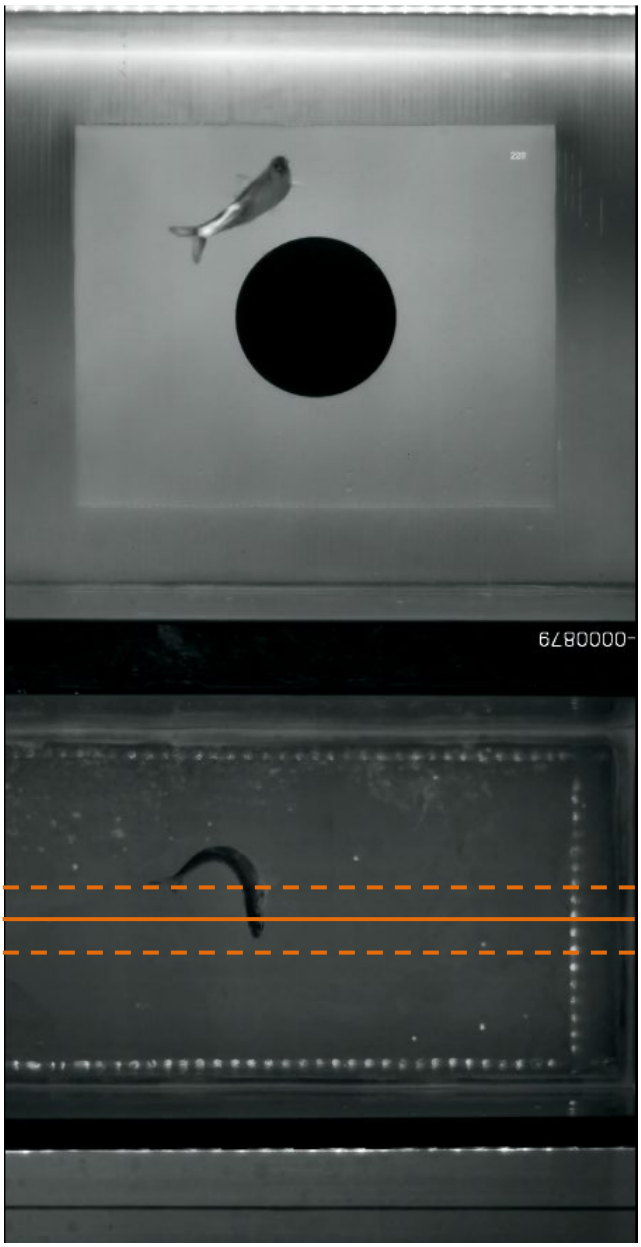

Movie S5- An anchovy (AF04 from Table S1) demonstrates a characteristic c-start escape response away from the stimulus when startled. High-speed cameras (250 Hz) allowed precise determination of the timing of response, and the frame number in the corner of the playback screen showed the stage of the animation at which the response occurred. In the overhead view the stimulus playback screen is situated along the top of the frame, the thick line was added to this image to represent the middle of the tank (16 cm from the screen), and the dotted lines represent the screen distance range (± 3 cm) at which a fish's response must occur to be counted in our analysis.

Supplemental code

The following scripts are available for download at:
https://purl.stanford.edu/mt574ws5287

Code S1 (in R and Matlab) to create the looming stimulus based on predator size, speed and engulfment timing

Code S2 (Matlab) to calculate energetic output of a lunge-feeding whale from speed and engulfment timing

Supplemental References

1. Cade DE, Carey N, Domenici P, Potvin J, & Goldbogen JA (2019) Data for "Predator-informed looming stimulus experiments reveal how large filter feeding whales capture highly maneuverable forage fish". Stanford Digital Repository. (https://purl.stanford.edu/mt574ws5287).
2. Cade DE, Friedlaender AS, Calambokidis J, & Goldbogen JA (2016) Kinematic Diversity in Rorqual Whale Feeding Mechanisms. *Current Biology* 26(19):2617-2624.
3. Goldbogen JA*, et al.* (2017) Using Digital Tags With Integrated Video and Inertial Sensors to Study Moving Morphology and Associated Function in Large Aquatic Vertebrates. *The Anatomical Record* 300(11):1935-1941.
4. Johnson MP & Tyack PL (2003) A digital acoustic recording tag for measuring the response of wild marine mammals to sound. *IEEE Journal of Oceanic Engineering* 28(1):3-12.
5. Cade DE, Barr KR, Calambokidis J, Friedlaender AS, & Goldbogen JA (2018) Determining forward speed from accelerometer jiggle in aquatic environments. *Journal of Experimental Biology* 221(2):jeb170449.
6. Batty R (1989) Escape responses of herring larvae to visual stimuli. *Journal of the Marine Biological Association of the United Kingdom* 69(3):647-654.
7. Dill LM (1974) The escape response of the zebra danio (Brachydanio rerio) I. The stimulus for escape. *Animal Behaviour* 22(3):711-722.
8. Faulk CK, Fuiman LA, & Thomas P (1999) Parental exposure to ortho, para-dichlorodiphenyltrichloroethane impairs survival skills of Atlantic croaker (*Micropogonias undulatus*) larvae. *Environmental toxicology and chemistry* 18(2):254-262.
9. Hein AM, Gil MA, Twomey CR, Couzin ID, & Levin SA (2018) Conserved behavioral circuits govern high-speed decision-making in wild fish shoals. *Proceedings of the National Academy of Sciences* 115(48):12224-12228.
10. Paglianti A & Domenici P (2006) The effect of size on the timing of visually mediated escape behaviour in staghorn sculpin *Leptocottus armatus*. *Journal of Fish Biology* 68(4):1177-1191.
11. Kahane-Rapport SR & Goldbogen JA (2018) Allometric scaling of morphology and engulfment capacity in rorqual whales. *Journal of Morphology*:1-13.

12. Horodysky AZ, Brill RW, Crawford KC, Seagroves ES, & Johnson AK (2013) Comparative visual ecophysiology of mid-Atlantic temperate reef fishes. *Biology open* 2(12):1371-1381.
13. Horodysky AZ, Brill RW, Warrant EJ, Musick JA, & Latour RJ (2008) Comparative visual function in five sciaenid fishes inhabiting Chesapeake Bay. *Journal of Experimental Biology* 211(22):3601-3612.
14. Hedrick TL (2008) Software techniques for two-and three-dimensional kinematic measurements of biological and biomimetic systems. *Bioinspiration & biomimetics* 3(3):034001.
15. Domenici P & Blake R (1997) The kinematics and performance of fish fast-start swimming. *Journal of Experimental Biology* 200(8):1165-1178.
16. Webb PW (1984) Body form, locomotion and foraging in aquatic vertebrates. *American zoologist* 24(1):107-120.
17. Temizer I, Donovan JC, Baier H, & Semmelhack JL (2015) A visual pathway for looming-evoked escape in larval zebrafish. *Current Biology* 25(14):1823-1834.
18. Hatsopoulos N, Gabbiani F, & Laurent G (1995) Elementary computation of object approach by a wide-field visual neuron. *Science* 270(5238):1000-1003.
19. Preuss T, Osei-Bonsu PE, Weiss SA, Wang C, & Faber DS (2006) Neural representation of object approach in a decision-making motor circuit. *Journal of Neuroscience* 26(13):3454-3464.
20. Domenici P (2001) The scaling of locomotor performance in predator–prey encounters: from fish to killer whales. *Comparative Biochemistry and Physiology Part A: Molecular & Integrative Physiology* 131(1):169-182.
21. Bainbridge R (1960) Speed and stamina in three fish. *Journal of Experimental Biology* 37(1):129-153.
22. Ward AJ, Herbert-Read JE, Sumpter DJ, & Krause J (2011) Fast and accurate decisions through collective vigilance in fish shoals. *Proceedings of the National Academy of Sciences* 108(6):2312-2315.
23. Marras S, Batty RS, & Domenici P (2012) Information transfer and antipredator maneuvers in schooling herring. *Adaptive Behavior* 20(1):44-56.
24. Sharpe FA (2001) Social foraging of the Southeast Alaskan humpback whale, *Megaptera Novaeangliae*. Ph.D. Dissertation (Simon Fraser University, Burnaby, B.C.).
25. Domenici P, Blagburn JM, & Bacon JP (2011) Animal escapology I: theoretical issues and emerging trends in escape trajectories. *Journal of Experimental Biology* 214(15):2463-2473.
26. Domenici P & Batty RS (1997) Escape behaviour of solitary herring (Clupea harengus) and comparisons with schooling individuals. *Marine Biology* 128(1):29-38.
27. Domenici P & Batty RS (1994) Escape manoeuvres of schooling Clupea harengus. *Journal of Fish Biology* 45(sA):97-110.
28. Franco-Moreno R-A*, et al.* (2015) Variability and sexual dimorphism in skull morphometry of California Sea Lions (Zalophus californianus) in Mexico. *Mammalian Biology* 80(4):316-327.
29. Godfrey SJ (1985) Additional observations of subaqueous locomotion in the California Sea Lion (*Zalophus californianus*). *Aqu. Mamm* 11:53-57.

30. Feldkamp SD (1987) Swimming in the California sea lion: morphometrics, drag and energetics. *Journal of Experimental Biology* 131(1):117-135.
31. Potvin J, Cade DE, Werth AJ, Shadwick RE, & Goldbogen JA (*in review*) Gigantism and the Energetics of Lunge-Feeding Baleen Whales. *Relevant portion available pre-publication at the Stanford digital repository: https://purl.stanford.edu/mt574ws5287*.
32. Webb PW (1971) The swimming energetics of trout: II. Oxygen consumption and swimming efficiency. *Journal of Experimental Biology* 55(2):521-540.
33. Webb PW (1975) Hydrodynamics and energetics of fish propulsion. *Bulletin of the fisheries research board of Canada* 190:1-159.
34. Blake RW (1983) *Fish locomotion* (CUP Archive).
35. Fish FE (1993) Power output and propulsive efficiency of swimming bottlenose dolphins (Tursiops truncatus). *Journal of Experimental Biology* 185(1):179-193.
36. Fish FE (1998) Comparative kinematics and hydrodynamics of odontocete cetaceans: morphological and ecological correlates with swimming performance. *Journal of Experimental Biology* 201(20):2867-2877.
37. Goldbogen JA*, et al.* (2011) Mechanics, hydrodynamics and energetics of blue whale lunge feeding: efficiency dependence on krill density. *The Journal of Experimental Biology* 214(1):131-146.
38. Hemmingsen AM (1960) Energy metabolism as related to body size and respiratory surface, and its evolution. *Reports of the Steno Memorial Hospital (Copenhagen)* 13:1-110.
39. Pyenson ND (2017) The Ecological Rise of Whales Chronicled by the Fossil Record. *Current Biology* 27(11):R558-R564.
40. Rodríguez-Romero J, Palacios-Salgado D, López-Martínez J, Hernández Vázquez S, & Velázquez-Abunader J (2009) The length–weight relationship parameters of demersal fish species off the western coast of Baja California Sur, Mexico. *Journal of Applied Ichthyology* 25(1):114-116.
41. Pitcher T & Partridge B (1979) Fish school density and volume. *Marine Biology* 54(4):383-394.
42. Domenici P, Batty RS, & Similä T (2000) Spacing of wild schooling herring while encircled by killer whales. *Journal of Fish Biology* 57(3):831-836.
43. Tirelli V*, et al.* (2006) Energy density of anchovy Engraulis encrasicolus L. in the Adriatic Sea. *Journal of Fish Biology* 68(3):982-989.
44. Dubreuil J & Petitgas P (2009) Energy density of anchovy *Engraulis encrasicolus* in the Bay of Biscay. *Journal of Fish Biology* 74(3):521-534.
45. Goldbogen JA*, et al.* (2008) Foraging behavior of humpback whales: kinematic and respiratory patterns suggest a high cost for a lunge. *Journal of Experimental Biology* 211(23):3712-3719.
46. Ydesen KS*, et al.* (2014) What a jerk: prey engulfment revealed by high-rate, super-cranial accelerometry on a harbour seal (*Phoca vitulina*). *Journal of Experimental Biology* 217(13):2239-2243.
47. Chenoweth EM (2018) *Bioenergetic and economic impacts of humpback whale depredation at salmon hatchery release sites* (University of Alaska Fairbanks).